Structure, excitations and probes of solids

Connect microscopic symmetry and dynamics to a measurement of a real solid. Develop the derivation and identify which experimental assumptions are needed to interpret the signal.

Contents

1. **Which reciprocal-lattice points produce a diffraction spot?**
   A bright spot depends on the wavelength and orientation of an incident beam, on the periodic repeat of a crystal, and on the atoms inside one repeat. Separate these three conditions so that a missing reflection becomes an interpretable observation. Then use the relative strength of two spots to estimate chemical order.
2. **Read atomic motion from Bragg attenuation and diffuse scattering**
   A crystal can retain its periodic mean positions while its diffraction pattern changes markedly with temperature. Start with the thermal average of a scattering amplitude, derive the displacement factor and learn which component of atomic motion a given reflection measures.
3. **Construct allowed bands from a cell transfer matrix**
   In a finite well a bound level follows from matching its wavefunction at the two walls. A periodic lattice replaces those two external walls by a matching condition on every cell. Derive a band criterion that works without guessing a wave inside the forbidden gap and use it to predict transmission through a finite sequence of cells.
4. **Why a large joint density of states can leave a dark optical edge**
   A band diagram gives the energy an electron needs to move between bands. It does not by itself tell whether light couples those states. Construct a two-orbital model with an explicit velocity operator, calculate its allowed and suppressed transitions, and distinguish electronic band curvature from optical selection rules.
5. **Count vacancies and infer an atomic migration barrier**
   Tracer atoms spread through a crystal even when the average lattice positions remain fixed. The rate can depend both on the number of vacant sites and on how readily an atom jumps into one. Derive the two factors separately, then compare an equilibrated specimen with a rapidly quenched one.
6. **Measure a phonon mean free path without confusing it with a sample length**

A cold insulating bar can carry heat primarily through lattice vibrations. Heat capacity tells how much energy the vibrations can carry; conductivity also depends on how far and in which direction they carry it. Derive the connection, test its limiting regimes, and identify when a measured thermal resistance belongs to a boundary.

7. A field profile that distinguishes a superconductor from a perfect conductor

Zero dc resistance tells how a current can persist. Field expulsion tells how a specimen responds when it enters a superconducting equilibrium state. Derive the London length, calculate what a finite slab and a thin film actually screen, and connect magnetic and electrical measurements to the same superfluid density.

8. Infer a superconducting gap from a tunnelling spectrum

A tunnel junction reports differential conductance versus voltage. Extracting a superconducting energy gap requires connecting a condensate's quasiparticle dispersion to a density of states, then accounting for temperature and finite spectral resolution before comparing peaks with the data.

9. Read twist and mismatch from the moiré of two lattices

Stack two square grids that differ slightly in orientation or pitch. The slowly varying registry map is visible over many unit cells. Derive its scale and direction in reciprocal space, and find which combinations of layer parameters a single period measurement can resolve.

10. From bonding energy to lattice spacing and sound speeds

Diffraction gives a spacing and ultrasound gives a stiffness. One measures where an energy curve is stationary, the other measures its curvature. Building the simplest energy of an ionic solid gives both observables and shows which quantities a spring model has already assumed.

11. Collective charge oscillations, bound excitons and lattice-dressed electrons

A loss peak in an electron spectrum, a line below an optical gap and an enhanced carrier mass call for different kinds of excitations. Start each model with its moving charges and its restoring interaction. That identifies what a measurement can determine.

12. Ferromagnetic resonance from angular momentum and free-energy curvature

A uniformly magnetised thin specimen can absorb microwave power at a frequency far from the bare spin Larmor frequency. The precessing magnetic moment creates its own field. Its geometry and the anisotropy determine which restoring torques appear in the measured resonance.

13. Lattice dislocations and structure without long-range order

A missing atom, a slipped lattice plane and a glass can all broaden a measurement, through very different mechanisms. Geometry distinguishes a line defect from a local vacancy. Correlation functions make the distinction between short-range order and crystallinity quantitative.

14. Why some alloys demix while others order on two sublattices

A binary alloy can cease to look random by separating into compositionally distinct regions or by arranging unlike atoms on alternating sites. A free energy for composition answers the first question. A second order parameter is needed for the second.

15. What extremal Fermi-surface orbits reveal about a metal

A single magnetic oscillation frequency gives one area in reciprocal space. Many different surfaces can share that area. Rotating the field and following how quantum oscillations and conductivity change turns the measurement into a three-dimensional inference problem.

Structure, excitations and probes of solids · 1. Which reciprocal-lattice points produce a diffraction spot?

A bright spot depends on the wavelength and orientation of an incident beam, on the periodic repeat of a crystal, and on the atoms inside one repeat. Separate these three conditions so that a missing reflection becomes an interpretable observation. Then use the relative strength of two spots to estimate chemical order.

Add amplitudes before squaring

Let an incident plane wave have wavevector $\mathbf{k}_i$ and the detected far-field direction select $\mathbf{k}_f$. Elastic scattering gives

$$|\mathbf{k}_i| = |\mathbf{k}_f| = 2\pi/\lambda.$$

In the single-scattering approximation a point at $\mathbf{r}$ contributes phase $(\mathbf{k}_i - \mathbf{k}_f)\cdot\mathbf{r}$. Define $\mathbf{Q} = \mathbf{k}_f - \mathbf{k}_i$; reversing the sign of all phases leaves the usual real-scatterer intensity invariant. With site positions $\mathbf{R} + \mathbf{d}_j$ and atomic scattering factors f_j, the total amplitude factors into a lattice sum over $\mathbf{R}$ and a basis structure factor $F(\mathbf{Q}) = \sum_j f_j(\mathbf{Q}) e^{-i\mathbf{Q}\cdot\mathbf{d}_j}$. Intensity is proportional to the squared magnitude of their product.

In a row of N sites of spacing a the lattice sum is a finite geometric series. Its intensity factor is $\sin^2(NQ_x a/2)/\sin^2(Q_x a/2)$, with value N^2 at an exact reciprocal point. The first zeros lie $2\pi/(Na)$ away from the maximum, so increasing the illuminated coherent length sharpens the spots. The area under an individual one-dimensional peak grows roughly linearly with N; the increase of peak height is accompanied by decreasing width. Comparing the height of an unresolved peak with an integrated intensity from another instrument can confuse finite domain size with a structural change.

Impose the Ewald condition and identify systematic absences

A reciprocal vector $\mathbf{G}$ produces a geometric reflection if $\mathbf{k}_f = \mathbf{k}_i + \mathbf{G}$ also lies on the elastic sphere. Squaring gives

$$2\mathbf{k}_i \cdot \mathbf{G} + G^2 = 0.$$

The reciprocal lattice point must lie on a sphere of radius k centred at $-\mathbf{k}_i$ in reciprocal coordinates. Rotating the crystal changes which points cross the sphere without changing their lengths. For plane spacing $d = 2\pi/G$, this condition gives

$$2d\sin\theta = \lambda,$$

with 2θ the angle between incident and outgoing beams. Geometric access requires $G \le 2k$; extending detector angle cannot violate the wavelength limit.

Now take a simple cubic repeat of side a with one site at $(0,0,0)$ and a second at $(a/2, a/2, a/2)$. For index (h,k,l),

$$F = f_A + (-1)^{h+k+l} f_B.$$

Even sums add, odd sums subtract. If the scatterers are identical the odd family vanishes: the apparent cubic description represented a body-centred Bravais lattice. If A and B are chemically distinct a corresponding odd spot can be visible. Its small intensity need not indicate a small lattice or poor alignment. The structural question is why a reciprocal point that satisfies the Ewald condition has small basis amplitude.

For $a = 0.400\,\mathrm{nm}$ and $\lambda = 0.154\,\mathrm{nm}$, a powder permits the (100) and (110) orientations. Their predicted 2θ positions are about 22.2° and 31.6°. If one replaces the scattering factors by constants $f_A = 28$, $f_B = 14$ for an illustrative comparison, odd-to-even squared amplitudes give

$$14^2/42^2 = 1/9.$$

The raw integrated powder peaks need not obey that ratio: multiplicity, angular geometry, polarisation, absorption, thermal attenuation and Q variation of atomic form factors also enter. Use corrected structure factors or compare symmetry-related measurements controlling those factors before converting a ratio into atomic contrast.

Infer partial chemical order and distinguish noise from disorder

Let half the atoms be species A and half B. On sublattice one, let probabilities for A, B be $(1+S)/2, (1-S)/2$; reverse them on sublattice two. $S = 1$ denotes complete order in the chosen assignment, $S = 0$ random mean occupancies. The average factors are $\bar{f}_1 = (f_A + f_B)/2 + S(f_A - f_B)/2$ and $\bar{f}_2 = (f_A + f_B)/2 - S(f_A - f_B)/2$. Thus the coherent odd Bragg amplitude is $S(f_A - f_B)$, while the even amplitude stays $f_A + f_B$. For equal domains and corrected geometry the ratio falls as S^2. Disorder may generate diffuse intensity away from Bragg peaks; its angular correlations contain information absent from the average occupancies.

If the corrected odd-to-even intensity ratio is 0.0400 for the stated $28 : 14$ contrast, $|S| = 0.600$. The magnitude alone cannot distinguish exchange of the two sublattices: S and $-S$ differ by an origin choice in this ideal case and lead to the same intensity. If relative intensity uncertainty is ten percent, the relative uncertainty of $|S|$ from that measurement is about five percent before scattering-factor and correction uncertainty. Near $S = 0$ a background subtraction or weak multiple scattering can dominate the inferred value. Report an upper limit when a corrected odd peak is consistent with the background.

Predict spots before changing the wavelength

The live calculation holds the cubic spacing and two scattering factors fixed, varies order and wavelength, and shows the resulting allowed powder-line positions and approximate strengths. The curves use a common artificial instrumental broadening to make discrete lines visible. Set $S = 0$ and identify which set survives. Restore order and alter wavelength; visible lines move because the Ewald

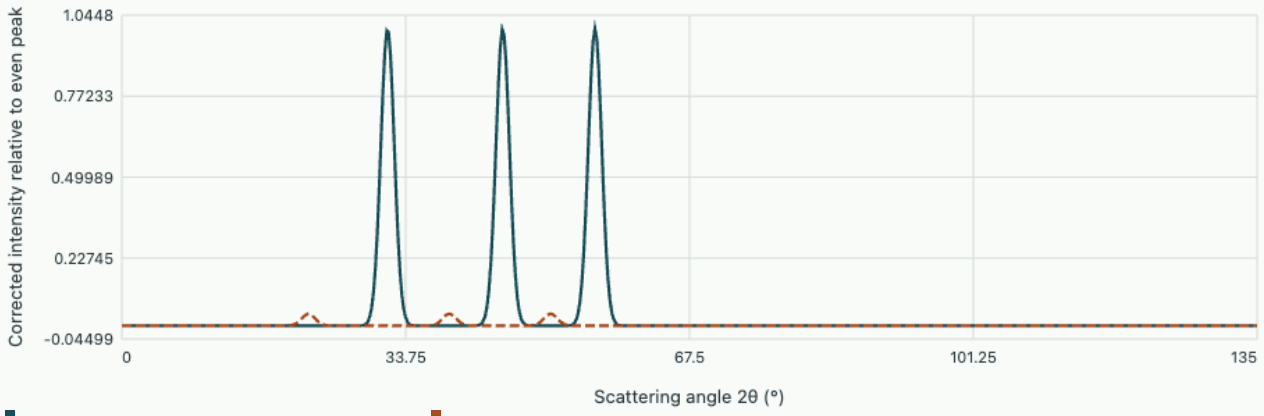
geometry changes, whereas the parity rule itself remains. At a large wavelength some high-index lines leave the accessible angular interval entirely. A disappearing peak caused by this scan is physically distinct from a basis extinction at the same index.

Open this experiment online

Try the calculation

Chemical order S **0.6**

Vacuum wavelength (nm) **0.154**



Even sum (selected families) Odd sum (selected families)

The corrected odd/even line ratio is 0.0400. The (100) and (110) geometric positions are 22.20° and 31.59°. Multiplicity and instrument response are excluded.

Compare a single-crystal rocking scan with a powder ring

An oriented single crystal at fixed wavelength generally places only a few reciprocal points near the Ewald sphere. Rotate it by a small angle about an axis transverse to the scattering plane and record intensity as one selected point sweeps through the sphere. Finite beam divergence, wavelength spread, mosaic block orientations and finite sample dimensions all broaden this rocking curve. A powder already contains crystallites with many orientations, so a matched spacing creates a ring; its integrated population is determined by the orientation distribution and multiplicity. A texture that aligns particular crystallites can strengthen or weaken one powder family without changing the underlying atomic structure factor.

An instructive control compares two samples cut from the same single crystal, one thick and one thin in the direction of the measured reciprocal vector. If the smaller coherent size is the main broadening mechanism, the reciprocal width should grow approximately inversely with thickness while the centre remains fixed. A distribution of lattice spacing produces a relative radial width that often increases with the magnitude of $\mathbf{G}$. Map both rocking and radial scans where possible, and measure an instrument standard. These independent directions distinguish a spread of orientations from a spread of spacings more effectively than fitting one width with an assumed coherent-domain formula.

Tutorial on geometric and structural tests

A corrected (100) intensity falls by a factor four after heating, while its corrected (110) intensity stays unchanged in the basic order model. What follows and what independent measurement should accompany it?

▼ **Work through the solution**

The absolute value of the order parameter halves because the odd line scales as S^2. Check more than one odd and even line and measure their angular widths and positions. Thermal motion generally attenuates high-Q intensities and a phase transition may change cell dimensions or domain size. A single ratio alone cannot separate every one of those effects.

For a cubic lattice $a = 0.400\,\mathrm{nm}$, can a wavelength $0.300\,\mathrm{nm}$ access the $(3, 0, 0)$ reflection by rotating the sample?

▼ **Work through the solution**

Its plane spacing is $0.1333\,\mathrm{nm}$, so even at backscattering $2d = 0.2667\,\mathrm{nm} < \lambda$. No rotation satisfies the elastic Ewald condition. Changing composition to increase the odd structure factor will not create a reflection at this wavelength. Shorten the wavelength or select a longer-spacing family.

Two samples have the same peak positions; one has a broader but lower central maximum. Does that establish a different lattice spacing?

▼ **Work through the solution**

Peak-centre position is what fixes spacing for a known wavelength. A finite coherent domain broadens peaks with width of order the inverse domain size. Microstrain or instrumental broadening can also broaden peaks. Measure the integrated line shape, a standard of known width, and several reciprocal vectors. Distinct causes of reduced peak height can then be separated from a change in mean lattice spacing.

David Tong derives real and reciprocal lattices in his Cambridge band-structure course.

Structure, excitations and probes of solids · 2. Read atomic motion from Bragg attenuation and diffuse scattering

A crystal can retain its periodic mean positions while its diffraction pattern changes markedly with temperature. Start with the thermal average of a scattering amplitude, derive the displacement factor and learn which component of atomic motion a given reflection measures.

Average a phase associated with a fluctuating position

Let an atom have position $\mathbf{R}+\mathbf{u}$, where $\mathbf{R}$ is its mean position and $\langle \mathbf{u} \rangle = 0$. At momentum transfer $\mathbf{Q}$, the coherent elastic amplitude is proportional to $e^{i\mathbf{Q}\cdot\mathbf{R}}\langle e^{i\mathbf{Q}\cdot\mathbf{u}} \rangle$. For a Gaussian displacement distribution with covariance $U_{ij} = \langle u_i u_j \rangle$, the scalar $X = \mathbf{Q}\cdot\mathbf{u}$ is Gaussian with zero mean and variance $Q_i U_{ij} Q_j$. Completing the square in its characteristic-function integral gives

$$\langle e^{iX} \rangle = e^{-\langle X^2 \rangle / 2}.$$

Thus the amplitude is multiplied by $e^{-Q_i U_{ij} Q_j/2}$; its coherent Bragg intensity receives the factor $e^{-Q_i U_{ij} Q_j}$ for equivalent atoms. Writing amplitude and intensity separately avoids the common factor of two error.

For isotropic motion the mean square displacement along one specified axis is U, with total three-dimensional mean square displacement $3U$. The intensity factor is $e^{-Q^2 U}$, not e^{-3Q^2U}. Crystallographic displacement notation often uses $B_{\mathrm{iso}} = 8\pi^2 U$, a quantity of dimension length squared unrelated to magnetic induction. With $Q = 4\pi \sin\theta/\lambda$, the amplitude factor can be written $e^{-B_{\mathrm{iso}} \sin^2\theta/\lambda^2}$. Different sources quote the exponent for amplitude or intensity, so determine which observable is being fitted before comparing reported displacement parameters.

Derive the thermal motion of one harmonic mode

For a one-dimensional harmonic displacement of mass M and angular frequency ω, quantisation gives

$$\hat{u} = \sqrt{\hbar/(2M\omega)}\,(a + a^\dagger).$$

In a number state the terms a^2 and $(a^\dagger)^2$ have zero expectation, while $aa^\dagger + a^\dagger a = 2n+1$. Thermal averaging with $\bar{n} = (e^{\hbar\omega/k_B T} - 1)^{-1}$ yields

$$\langle u^2 \rangle = \frac{\hbar}{2M\omega} \coth \frac{\hbar\omega}{2k_B T}.$$

At low temperature the mode retains a zero-point contribution independent of temperature. At high temperature $\coth x \simeq 1/x$ gives $k_B T/(M\omega^2)$, the equipartition result for the quadratic potential. Light atoms and soft modes can therefore show substantial positional fluctuations. A real crystal contains modes with different polarisations, frequencies and atomic amplitudes; a single fitted Einstein frequency is a model of their weighted contribution, not automatically the frequency of one identifiable phonon.

For illustrative $M = 40$ atomic mass units and ordinary frequency $f = 5.0\,\mathrm{THz}$, $\hbar\omega/k_B$ is about $240\,\mathrm{K}$. The one-mode zero-point variance is about $2.53 \times 10^{-23}\,\mathrm{m}^2 = 0.00253\,\mathrm{\AA}^2$. At $300\,\mathrm{K}$ the multiplier $\coth(0.40)$ is about 2.63, so the rms displacement grows from $0.0503\,\mathrm{\AA}$ to $0.0816\,\mathrm{\AA}$. At $Q = 8.0\,\mathrm{\AA}^{-1}$ the corresponding intensity factors are about 0.850 and 0.654. Atomic motion still much smaller than an interatomic spacing can therefore noticeably attenuate a high-angle peak.

Infer a covariance change and interpret missing intensity

For the same reflection at two temperatures, after scale, form factor, absorption, structural order and other changes have been corrected,

$$\ln[I_2/I_1] = -Q_i \Delta U_{ij} Q_j.$$

In an isotropic crystal plot this logarithm against Q^2. The slope estimates negative ΔU; a nonzero intercept can indicate a relative monitor or normalisation change. With $I_2/I_1 = 0.80$ at $Q = 6.0\,\mathrm{\AA}^{-1}$,

$$\Delta U = 0.00620\,\mathrm{\AA}^2.$$

This determines a variance difference, not the rms at either temperature individually. Simply taking the square root of a variance difference and calling it the rms increase generally gives the wrong quantity.

For anisotropic fluctuations the measurement probes a quadratic form. Reflections along three crystallographic axes constrain the diagonal elements, while an off-axis vector also depends on cross terms such as $2Q_xQ_yU_{xy}$. A full covariance must be positive semidefinite. A refinement returning a negative directional variance may indicate insufficient angular coverage, a wrong model or strongly correlated fitting parameters. Symmetry of site occupation can reduce the number of independent covariance components; an analysis with more unconstrained parameters than informative reflections risks interpreting noise as a preferred vibration axis.

Diffuse scattering clarifies what has happened to the lost coherent intensity. For a given configuration the measured intensity is the squared sum of amplitudes. Its thermal expectation can be split into the squared mean amplitude plus the variance of fluctuations about that mean. Correlated displacements between atoms contribute structured diffuse intensity, especially near Bragg positions. An instrument integrating a wide region around a peak can inadvertently include temperature-dependent diffuse background and underestimate the attenuation of the coherent peak. Energy-resolved scattering can separate elastic peaks from inelastic phonon scattering more directly than a simple static intensity ratio.

Reconstruct an off-axis displacement correlation

Suppose calibrated temperature-difference measurements in an orthogonal x, y plane give

$$\Delta U_{xx} = 0.0040\ \text{Å}^2,$$

$$\Delta U_{yy} = 0.0080\ \text{Å}^2.$$

Along a direction halfway between the axes the inferred projection variance is $0.0075\ \text{Å}^2$. For $\hat{n} = (1,1)/\sqrt{2}$, the directional variance is $(\Delta U_{xx} + \Delta U_{yy})/2 + \Delta U_{xy}$. Thus the cross covariance is $+0.0015\ \text{Å}^2$. The direction $(1,-1)/\sqrt{2}$ should give $0.0045\ \text{Å}^2$. A scan of both diagonals cancels the trace term in their difference and isolates twice the off-diagonal covariance directly.

At $Q = 8\ \text{Å}^{-1}$ these two diagonal directions predict hot-to-cold ratios $e^{-64(0.0075)} = 0.619$ and $e^{-64(0.0045)} = 0.750$. An isotropic fit to their average would conceal this significant angular difference. If only one orientation is measurable due to sample mounting, symmetry constraints or a second mounting angle can supply missing information. The two eigenvalues of the illustrative covariance difference are 0.0035 and $0.0085\ \text{Å}^2$, both positive. In general the absolute covariance at every temperature must be positive semidefinite, while a difference of two positive covariances need not be positive along every axis. A structural change on heating can reduce fluctuations along one direction while increasing them along another.

Compare a temperature difference with an absolute structure refinement

An unknown constant site displacement and an unknown absolute intensity scale make a single-temperature fit less direct than a temperature ratio. On heating, measure both a small-Q reflection and a high-Q reflection in rapid alternation with a fixed incident monitor. Slow detector gain variation then affects the two less differently. If both corrected ratios fall equally, a scale change is more plausible than an added Gaussian displacement factor, which predicts a stronger effect at larger Q^2. Repeating over several independent directions tests that conclusion against anisotropic motion.

Tutorial on a temperature scan

Two equivalent high-symmetry reflections have $Q = 4$ and $8\ \text{Å}^{-1}$. Their corrected hot-to-cold ratios are 0.92 and 0.72. Are these consistent with a common isotropic variance change?

▼ **Work through the solution**

Individually they give

$$-\ln 0.92/16 = 0.00521,$$

$$-\ln 0.72/64 = 0.00513\ \text{Å}^2.$$

The close results are consistent within modest intensity uncertainties. Agreement across two points does not establish isotropy in all directions; add noncollinear reflections and check the fitted scale

offset.

A fit reports an rms displacement of $0.10\ \text{Å}$ along each of three independent axes. What is the expected coherent intensity fraction at $Q = 10\ \text{Å}^{-1}$, and what is the total rms distance from the mean site?

▼ **Work through the solution**

Each directional variance is $0.010\ \text{Å}^2$. The fraction is

$$e^{-1} = 0.368.$$

The rms length of the three-dimensional displacement vector is

$$\sqrt{0.030} = 0.173\ \text{Å}.$$

The projection onto the scattering vector uses one directional variance, while total rms length sums all three.

An isotropic displacement fit stays large at the lowest measured temperature. What measurements distinguish static disorder from zero-point motion?

▼ **Work through the solution**

A constant displacement contribution can arise from both an unresolved distribution of mean site positions and quantum fluctuations. Extend the temperature range, compare isotopes or mode frequencies where feasible, and measure diffuse scattering with energy resolution. A harmonic calculation with independently measured phonon frequencies predicts a zero-point scale. Absolute Bragg attenuation alone gives a distribution width without uniquely identifying its microscopic source.

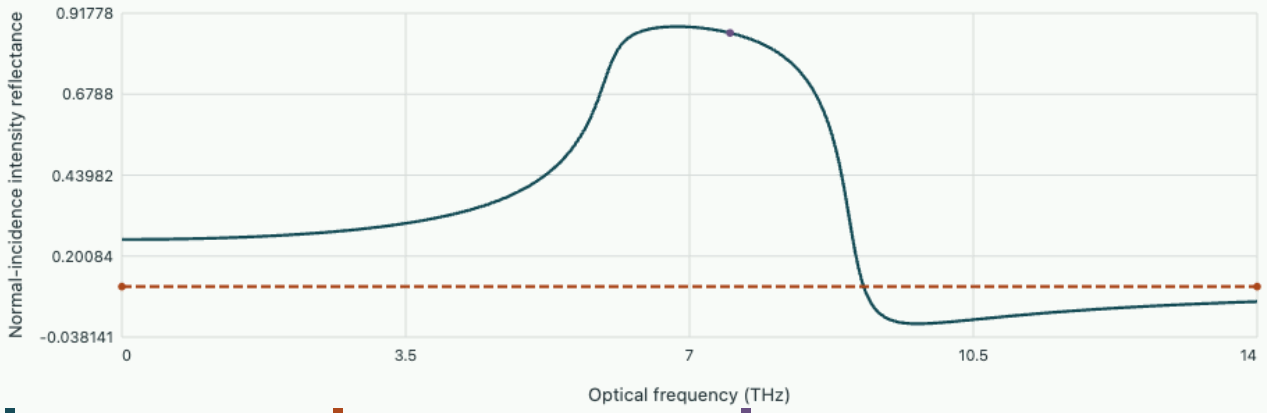
The International Union of Crystallography examines the displacement factors entering a diffraction intensity.

Compare the dynamics of a polar lattice mode with a static displacement measurement.

Open this experiment online

Try the calculation

Static relative permittivity	**9**
Damping ratio γ/ωTO	**0.05**
Probe frequency (THz)	**7.5**



Damped ionic crystal Electronic background only Selected frequency

Lossless TO pole 6 THz and LO zero 9 THz. At 7.5 THz the chosen damping gives reflectance 0.8596.

Structure, excitations and probes of solids · 3. Construct allowed bands from a cell transfer matrix

In a finite well a bound level follows from matching its wavefunction at the two walls. A periodic lattice replaces those two external walls by a matching condition on every cell. Derive a band criterion that works without guessing a wave inside the forbidden gap and use it to predict transmission through a finite sequence of cells.

Transfer a wave and its derivative through one interval

Consider a particle of mass m in a one-dimensional array of repulsive delta barriers $V(x) = g\sum_n \delta(x - na)$, with $g > 0$ of units energy times length. Between barriers $E > 0$, so the Schrödinger equation becomes $\psi'' + k^2\psi = 0$, $k = \sqrt{2mE}/\hbar$. A solution over one empty interval maps the column (ψ, ψ') by a matrix with rows $(\cos ka, \sin ka/k)$ and $(-k\sin ka, \cos ka)$. Both value and derivative propagate; their units differ, as the factors of k show.

Integrate the Schrödinger equation across one narrow interval containing a delta barrier. The derivative jump is $\psi'_+ - \psi'_- = (2mg/\hbar^2)\psi$, while the wavefunction remains continuous. A barrier map therefore has unit diagonal, zero upper off-diagonal term and lower off-diagonal value $2mg/\hbar^2$. The determinant of each propagation map is one, reflecting conservation of the Wronskian. Multiplying barrier and free matrices gives the one-cell map M. Starting at a different point of the same periodic cell changes that matrix by a similarity transformation and leaves its trace and eigenvalues unchanged.

Derive the Bloch condition and identify a forbidden interval

A Bloch solution satisfies

$$(\psi, \psi')(x + a) = e^{iqa}(\psi, \psi')(x).$$

Therefore e^{iqa} is an eigenvalue of M; determinant one gives its partner e^{-iqa}. Half the trace is their average. Multiplying the two elementary matrices and introducing $x = ka$ and dimensionless barrier strength $P = mga/\hbar^2$ gives

$$\cos(qa) = F(x) = \cos x + P\frac{\sin x}{x}.$$

The free propagation wave number k defines the energy, while the Bloch wave number q specifies phase advance between equivalent cells. They coincide modulo reciprocal lattice vectors only in the unperturbed limit. A real q exists exactly when $|F| \le 1$. If $|F| > 1$, q must be complex; field magnitude changes exponentially from one cell to the next. A perfect infinite lattice then has no extended state at that energy, though a finite sample can support evanescent penetration from a contact.

For $P = 1$, $x = \pi/2$ gives

$$F = 2/\pi = 0.63662,$$

$$qa = \arccos(2/\pi) \simeq 0.881.$$

At $x = \pi$, $F = -1$ independent of P, a band edge. At $x = 3.40$, $F \approx -1.042$, inside a gap. Writing $q = \pi/a + i\kappa$ there gives $\cos qa = -\cosh(\kappa a)$, or $\kappa a = \operatorname{arcosh}|F| \approx 0.29$. A pure decaying solution falls by roughly $e^{-2.9}$ in amplitude over ten cells. A two-contact transmission measurement also depends on interface matching and admixtures of growing and decaying solutions; this envelope alone does not give the exact transmission probability.

Connect band edges to standing waves and curvature

At a zone edge the unperturbed right- and left-going states are degenerate. Their symmetric and antisymmetric combinations place maxima or nodes on the barriers. A sine standing wave with nodes at every barrier vanishes where the delta potential acts and retains its corresponding free energy. The complementary standing wave has nonzero barrier amplitude and shifts up. For small P, expand near $x = \pi + \delta$:

$$F \simeq -1 + \delta^2/2 - P\delta/\pi.$$

The two band edges with $F = -1$ are $\delta = 0$ and $\delta \simeq 2P/\pi$. Their energy separation is $\Delta E \simeq 2g/a$, since $E = \hbar^2 x^2/(2ma^2)$. This equals twice the magnitude of the first reciprocal-space Fourier amplitude of the periodic delta array, connecting the transfer-matrix and nearly-free-electron pictures.

Band curvature controls the acceleration of a slowly varying wave packet. Implicit differentiation gives $-a\sin(qa)\,dq/dE = dF/dE$ and hence

$$v_g = \hbar^{-1} dE/dq = -a\sin(qa)/[\hbar F'(E)].$$

At an ordinary edge $\sin qa = 0$, group velocity vanishes. Expanding both sides quadratically in the displacement of q shows the local effective mass can be positive at a lower minimum and negative at an upper maximum. Direct differentiation of a numerically sampled inverse cosine near its endpoint can amplify rounding error. Fitting $E(q)$ locally to a parabola and checking the interval used is generally more reliable.

Reconstruct a band diagram from the trace

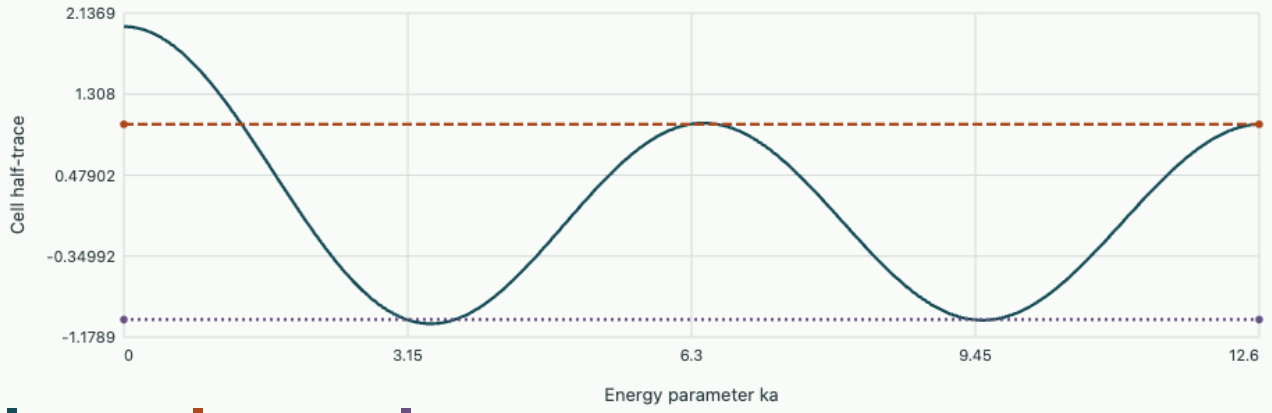
The live plot displays the half-trace as a function of energy parameter ka together with the boundaries at plus and minus one. Start with the free system and then raise P; identify where a previously tangential contact with $|F| = 1$ opens into an interval outside the allowed strip. Choose a test ka and read either the Bloch phase or the penetration length. Changing a at fixed P, ka rescales the physical energy as a^{-2}. A real scan of lattice spacing at fixed barrier strength g also changes P, so it cannot generally be represented by shifting only the horizontal energy labels.

Open this experiment online

Try the calculation

Barrier strength P **1**

Selected ka **3.4**



Half-trace at the selected energy is -1.0420. The decaying Bloch amplitude falls by 1/e in 3.46 cells.

Determine how a finite pass band produces resonant transmission

The trace controls a finite periodic sample as well as its infinite limit. For a determinant-one cell matrix the Cayley–Hamilton identity is

$$M^2 - 2FM + 1 = 0.$$

Repeatedly applying it gives

$$M^N = U_{N-1}(F)M - U_{N-2}(F)1,$$

with U_j the Chebyshev polynomials of the second kind. Inside a band $F = \cos qa$, so $U_{N-1} = \sin(Nqa)/\sin(qa)$. When $Nqa = j\pi$ strictly inside a band, the coefficient of M vanishes and the remaining total matrix is $(-1)^j 1$. With identical homogeneous leads on both sides this matches a travelling wave without reflection, giving a finite-stack transmission resonance even when one cell alone reflects substantially.

For six identical cells the candidate phases $qa = \pi/6, \ldots, 5\pi/6$ lie within each uncomplicated pass band. Their energies are found by solving the half-trace relation at each prescribed cosine; they are generally not equally spaced in energy. At a band edge $\sin qa = 0$ the divided expression appears singular, but the limiting polynomial remains finite. Exact transparency at the interior phases also assumes coherent propagation and accurately repeated barriers. Variations in cell strength, unequal external leads and inelastic dephasing alter the heights or positions. Comparing how the resonance

spacing changes with cell count distinguishes finite-stack resonances from a fundamental bulk band gap.

Check dimensions against a measured energy scale

For $a = 0.50\,\mathrm{nm}$ and bare electron mass, the zone-edge free energy $\hbar^2\pi^2/(2ma^2)$ is about $1.50\,\mathrm{eV}$. Doubling the repeat distance at fixed mass lowers this reference by a factor four. Thus a plotted gap width measured in ka cannot be quoted directly in electronvolts without the lattice spacing, mass and selected location on the nonlinear energy axis. Using a fitted effective mass already incorporating the same periodic potential can also double count its effect. State the degrees of freedom represented by the unperturbed kinetic term.

Tutorial on allowed and forbidden propagation

Why is there no extended zero-energy state for any positive barrier strength in this model?

▼ **Work through the solution**

As $x \to 0$, $\sin x/x \to 1$ and $F(0) = 1 + P > 1$. The bottom of the first allowed band is shifted upward from zero. A constant wavefunction would have nonzero values at the barriers but zero derivative jump, violating the jump condition. Removing the barriers gives $P = 0$ and restores the constant zero-energy state.

At an energy with $F = -1.10$, how many cells attenuate a purely evanescent amplitude by a factor of ten?

▼ **Work through the solution**

The inverse decay length in units of cells is $\operatorname{arcosh}(1.10) = 0.444$. Setting $e^{-N\cdot 0.444} = 0.10$ gives $N = 5.19$, so six complete cells reduce it by more than ten. Intensity decays with twice the exponent. The alternating Bloch phase associated with a negative trace does not reverse the exponential attenuation.

A numerically multiplied matrix after several thousand gap cells overflows. Does this invalidate the band calculation?

▼ **Work through the solution**

A lossless cell has reciprocal eigenvalues; in a gap one grows while the physical decaying solution shrinks. Direct multiplication amplifies roundoff in the growing direction. Recover the bulk exponent from the one-cell trace or use a stable scattering-matrix or logarithmic-derivative formulation for a

finite sample. Check conservation in an allowed band and compare the extracted decay exponent as the finite sample grows.

David Tong connects one-dimensional periodic-potential matching to Bloch bands.

Structure, excitations and probes of solids · 4. Why a large joint density of states can leave a dark optical edge

A band diagram gives the energy an electron needs to move between bands. It does not by itself tell whether light couples those states. Construct a two-orbital model with an explicit velocity operator, calculate its allowed and suppressed transitions, and distinguish electronic band curvature from optical selection rules.

Build a two-orbital Bloch Hamiltonian from parity

Consider one even and one odd orbital centred on each site of a one-dimensional chain of period a. Their onsite energies are $+\Delta$ and $-\Delta$. Suppose the only hopping retained mixes opposite orbital types on adjacent sites and has opposite signs to the left and right. Fourier transforming that difference gives a term proportional to $e^{ika} - e^{-ika} = 2i \sin ka$. Choosing orbital phases appropriately gives

$$H(k) = \Delta\sigma_z + 2t \sin(ka)\sigma_y.$$

This is a deliberately simple spinless two-band model with orthonormal, co-centred orbitals and a fixed basis. Physical multiorbital models can require additional intra-atomic dipole or position-matrix elements; here the optical coupling is defined through a uniform vector potential acting on the hopping phases.

Diagonalising a traceless Pauli-vector Hamiltonian gives

$$E_{\pm} = \pm E(k),$$

$$E(k) = \sqrt{\Delta^2 + 4t^2 \sin^2 ka}.$$

At half filling and zero temperature, the lower band is occupied and the upper is empty. A photon of visible-light wavelength usually has very small momentum compared with the size of a Brillouin zone in an atomic crystal. Neglecting its crystal momentum gives a vertical transition at fixed k with required energy $2E(k)$. This energetic condition defines a joint density of candidate states. A matrix element still determines their optical weight.

Derive the velocity matrix element before summing transitions

A uniform vector potential shifts the crystal wavevector in this tight-binding model, yielding velocity $v = \hbar^{-1}\partial_k H = (2ta/\hbar)\cos(ka)\,\sigma_y$. Let $\hat{\mathbf{d}} = (0, 2t\sin ka, \Delta)/E$. The upper eigenstate has $\langle +|\boldsymbol{\sigma}|+\rangle = \hat{\mathbf{d}}$. Insert the completeness relation $1 = |+\rangle\langle +| + |-\rangle\langle -|$ into $\langle +|\sigma_y^2|+\rangle = 1$. This gives

$$|\langle +|\sigma_y|-\rangle|^2 = 1 - \hat{d}_y^2 = \Delta^2/E^2.$$

Thus

$$|v_{+-}(k)|^2 = \left(\frac{2ta}{\hbar}\right)^2 \cos^2(ka)\,\frac{\Delta^2}{\Delta^2 + 4t^2\sin^2(ka)}.$$

At $ka = 0$ or π the interband velocity is maximal, even though the diagonal group velocity of either band is zero at these extrema. The optical matrix element connects different states; it is not the derivative of one eigenvalue. At $ka = \pi/2$ the interband velocity vanishes because the Hamiltonian has zero first derivative. The energy separation there is maximal and has zero slope as well. A state-counting argument alone would emphasise that band edge while the optical coupling suppresses it.

For $\Delta = 0.50\,\mathrm{eV}$, $t = 0.40\,\mathrm{eV}$, and $a = 0.40\,\mathrm{nm}$, transition energies range from 1.00 to $1.89\,\mathrm{eV}$. The velocity scale $2ta/\hbar$ is about $4.86 \times 10^5\,\mathrm{m/s}$. At $ka = \pi/4$, $E^2 = 0.25 + 0.32 = 0.57\,\mathrm{eV}^2$, so the squared matrix element in units of its zone-centre value is

$$0.5(0.25/0.57) = 0.219.$$

States at that wavevector contribute substantially less per state than at threshold even before differences in available state density or occupation are included.

Derive the line shape near the upper and lower edges

In a weak-field independent-electron model an interband spectral weight contains an integral $\int dk\,[f_-(k) - f_+(k)]|v_{+-}(k)|^2\delta[\hbar\omega - 2E(k)]$, together with known optical prefactors. For a simple root of $2E(k) = \hbar\omega$, the delta function contributes an inverse derivative $1/|2E'(k)|$. Near a quadratic one-dimensional extremum this factor grows as the inverse square root of the energy distance from the edge. That is the familiar van Hove feature in the unweighted joint density. One must multiply by the matrix element at precisely the same wavevector before interpreting it as absorption.

Near the lower edge write $ka = x \ll 1$. Then $2E \simeq 2|\Delta| + 4t^2x^2/|\Delta|$, and the squared velocity tends to a finite constant. The independent-particle absorption weight has an inverse-square-root onset in this ideal one-dimensional model. Near the upper edge put $ka = \pi/2 + s$ with small s. The distance from the maximum transition energy is proportional to s^2, but $|v_{+-}|^2 \propto s^2$. Multiplying this by the $1/|s|$ joint-density factor produces a weight that vanishes as a square root. The same quadratic band-edge geometry thereby creates entirely different optical signatures at the two edges.

Finite temperature modifies the occupations; moving the chemical potential into the upper band can block some low-energy transitions by Pauli exclusion. Lifetime and instrument broadening smear each edge. Electron–hole attraction can also create bound exciton peaks below the independent-particle onset. A measured absorption line below a band gap inferred from one-electron energies is therefore not automatically an error in the band calculation. Test how the feature changes with carrier density, temperature, polarisation and resolution before assigning its microscopic origin.

Distinguish a vertical transition from a phonon-assisted onset

If the valence maximum and conduction minimum occur at different crystal wavevectors, a direct vertical photon transition may require a larger energy than the minimum electronic gap. A lattice vibration can supply or remove the missing crystal momentum. Let the indirect gap be E_g, and suppose a phonon mode of energy $\hbar\omega_{\mathrm{ph}}$ connects the extrema. Phonon absorption provides part of the required

energy, so photon onset can occur near $E_g - \hbar\omega_{\mathrm{ph}}$, weighted by the occupation n_{ph}. Phonon emission costs energy and starts near $E_g + \hbar\omega_{\mathrm{ph}}$, weighted by $n_{\mathrm{ph}} + 1$. At low temperature the emission channel can remain while the phonon absorption channel weakens.

For $E_g = 1.10\,\mathrm{eV}$ and phonon energy $0.040\,\mathrm{eV}$, the simple channel edges are 1.06 and $1.14\,\mathrm{eV}$. At $300\,\mathrm{K}$ the Bose occupation is about 0.270, so the ratio of absorption to emission statistical factors is $n/(n+1) \approx 0.213$. Matrix elements and available electronic states also affect measured intensity, so the intensity ratio need not equal that number directly. Compare temperature and momentum dependence with an independently mapped electronic dispersion. A weak low-energy feature can reflect an indirect process rather than a symmetry-forbidden direct transition, two mechanisms that the direct one-dimensional model intentionally separates.

Check what reversing the hopping sign can reveal

Changing t to $-t$ in this restricted Hamiltonian leaves both band energies and the squared interband matrix element unchanged. A redefinition of one local orbital by a phase of π produces exactly that sign change. A fit to one absorption spectrum therefore cannot identify an absolute sign for this lone hopping. Relative phases among several independent paths can become observable through interference in a richer orbital model.

Tutorial on interpreting optical data

At equal density of candidate states for two selected small k intervals, the second interval has $ka = \pi/4$ and the first $ka = 0$. Which optical signal ratio does the model predict if occupancies and other prefactors are matched?

▼ **Work through the solution**

The answer is the squared velocity ratio 0.219 for the numerical parameters. A ratio of velocity magnitudes would give the square root of that value and would be inappropriate for a transition probability. In a direct frequency sweep the state-density factors at those two energies generally differ, so this particular comparison presupposes selected or separately corrected state intervals.

A numerical spectrum represents each delta function by a box of width Γ. How should a peak comparison be checked as Γ decreases?

▼ **Work through the solution**

Increase the k-mesh density so each bin contains enough states, especially near extrema where roots merge. Compare integrated weight over a fixed finite energy window and use broadening normalised to unit area. Then vary Γ separately from the mesh. Otherwise a disappearing or sharpening feature may reflect changing sample counts per bin instead of the true matrix element.

Can the model predict a strong direct transition simply because $2E(k)$ equals the photon energy at a band maximum?

▼ **Work through the solution**

The maximum at $ka = \pi/2$ is an explicit counterexample: its velocity matrix element vanishes. Additional allowed optical couplings or symmetry breaking in a real material can restore weight, so identify which perturbation the model includes. The band energies alone supply a necessary energetic condition and the matrix element supplies an independent condition on how the external field drives the transition.

Vary a two-band hopping model and distinguish its dispersion from the optical weights.

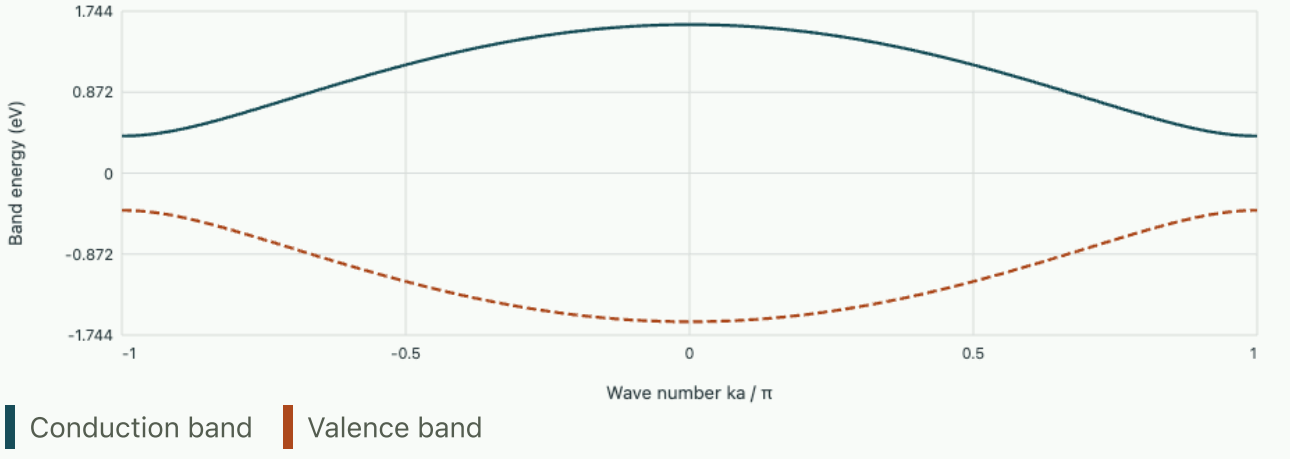
David Tong derives tight-binding Hamiltonians and electronic dynamics in solids.

Open this experiment online

Try the calculation

Intracell hopping t_1 (eV) **1**

Intercell hopping t_2 (eV) **0.6**



Direct gap 0.8 eV. Each band spans 1.2 eV.

Structure, excitations and probes of solids · 5. Count vacancies and infer an atomic migration barrier

Tracer atoms spread through a crystal even when the average lattice positions remain fixed. The rate can depend both on the number of vacant sites and on how readily an atom jumps into one. Derive the two factors separately, then compare an equilibrated specimen with a rapidly quenched one.

Minimise the free energy of a dilute vacancy population

Take N lattice sites and n equivalent vacancies, ignoring their interactions. The microscopic formation Gibbs free energy $G_f = H_f - TS_f$ includes local vibrational and other nonconfigurational changes associated with creating one defect and transferring the removed atom to an appropriate reservoir. The configurational multiplicity is $\binom{N}{n}$. Thus $G - G_0 = nG_f - k_BT \ln \binom{N}{n}$. Applying Stirling's approximation and differentiating with respect to n gives $G_f + k_BT \ln[n/(N-n)] = 0$, or $c_v/(1-c_v) = e^{-G_f/k_BT}$, where $c_v = n/N$. In the dilute limit $c_v \simeq e^{S_f/k_B} e^{-H_f/k_BT}$.

A positive formation enthalpy does not imply zero vacancies in thermal equilibrium. The number of ways to place a few defects contributes entropy. The dilute independent-site argument ceases to apply if vacancies cluster, interact strongly, or if charge neutrality ties their population to other charged defects. Specifying the atomic reservoir is especially important in compounds: removing a metal atom and removing a nonmetal atom are different chemical operations with potentially different energies and charge states. The present simple model describes one kind of neutral vacancy under fixed thermodynamic conditions.

For $H_f = 1.00\,\mathrm{eV}$, $S_f = k_B$ and $T = 800\,\mathrm{K}$, $k_BT = 0.06894\,\mathrm{eV}$ and $c_v \simeq 1.36 \times 10^{-6}$. A cubic micrometre containing an illustrative 5×10^{10} sites then contains about 6.8×10^{4} vacancies on average. The fraction is tiny while the count in a region accessible to a diffusion experiment can be large. In a nanocrystal with far fewer sites the mean can be much less than one; a single defect entering or leaving may then change the observed motion intermittently.

Derive a tracer diffusivity from correlated jumps

Let the coordination number be z, jump length d, and the conditional rate of one atom jumping into one specified neighbouring vacancy be $\Gamma = \nu_0 e^{-H_m/k_BT}$. For dilute, randomly located vacancies a tracer has on average zc_v vacant nearest neighbours and jump rate $zc_v\Gamma$. For an uncorrelated isotropic three-dimensional random walk $\langle |\Delta \mathbf{r}|^2 \rangle = zc_v\Gamma t\, d^2 = 6Dt$. Successive tracer jumps can be correlated because the vacancy just exchanged with it is now directly behind it. Introduce the cumulative correlation factor f to obtain

$$D = fzd^2\Gamma c_v/6.$$

The definition of Γ per specified neighbour matters: a tabulated total jump frequency already summed over neighbours must not acquire a second factor z.

Under the stated equilibrium assumptions the apparent Arrhenius activation energy of the tracer is $H_f + H_m$. The first term controls whether an opportunity to jump exists, the second controls the rate

at which an available opportunity is taken. At fixed excess vacancy concentration only the migration contribution enters to leading order if f and the prefactor stay nearly constant. This offers a way to separate the two barriers, provided the excess concentration persists during the measurement. A fitted straight line through data from specimens with different thermal histories is not automatically the property of one microscopic jump.

For $H_m = 0.50\,\mathrm{eV}$, $\nu_0 = 10^{13}\,\mathrm{s^{-1}}$, $z = 12$, $d = 0.25\,\mathrm{nm}$, $f = 0.78$ and the equilibrium vacancy fraction at $800\,\mathrm{K}$, one obtains $\Gamma \simeq 7.1 \times 10^{9}\,\mathrm{s^{-1}}$ and $D \simeq 9.4 \times 10^{-16}\,\mathrm{m^2/s}$. The apparent discrepancy between a gigahertz conditional jump rate and the slow macroscopic spreading comes largely from the small vacancy fraction. After one hour the rms spread in one Cartesian direction is $\sqrt{2Dt} \simeq 2.6\,\mu\mathrm{m}$; the three-dimensional rms displacement is larger by $\sqrt{3}$.

Read a diffusion measurement and identify a changing population

For a thin tracer layer deposited at the origin of a long homogeneous specimen the one-dimensional conservative diffusion equation gives

$$c(x,t) = M (4\pi D t)^{-1/2} e^{-x^2/(4Dt)},$$

where M is the deposited amount per area. Its variance is $2Dt$. An initial Gaussian width or an independent Gaussian instrument resolution adds its own variance. Measure the growth of variance with time to estimate D, instead of attributing the entire final width to diffusion. An asymmetric tail can signal surface or grain-boundary transport, which may not be described by a uniform bulk D.

Now quench a specimen rapidly from a higher temperature. Vacancies may initially remain near their high-temperature population while their mobility changes immediately. If their excess decays to sinks as $c_v(t) = c_{\mathrm{eq}} + c_{\mathrm{exc}} e^{-t/\tau_s}$, tracer spreading at fixed temperature follows $\sigma_x^2(t) - \sigma_x^2(0) = 2\int_0^t D(t')\,dt'$. If D is proportional to c_v, this consists of a linear equilibrium contribution and a saturating excess term proportional to $\tau_s(1 - e^{-t/\tau_s})$. A single long-time apparent diffusivity conceals early rapid motion. Measuring several dwell times and different specimen sizes can reveal the role of sinks.

Use unequal dwell times to test a quenched vacancy excess

Take a quenched specimen at fixed measuring temperature and suppose the excess initially raises the tracer diffusivity from its equilibrium value D_{eq} to $D_{\mathrm{eq}} + 3D_{\mathrm{eq}}$. Let excess vacancies decay with time constant $600\,\mathrm{s}$. A variance measurement over the first $300\,\mathrm{s}$ infers a time-averaged coefficient $D_{\mathrm{app}}/D_{\mathrm{eq}} = 1 + 3(600/300)[1 - e^{-300/600}] = 3.36$. The same calculation over the first $3600\,\mathrm{s}$ gives about 1.50. Neither averaged coefficient equals the initial fourfold value or the long-time equilibrium value. A collection of samples analysed after unequal dwell times can therefore seem to have different activation energies even at equal measurement temperatures.

Independent reheating or quenching measurements can help identify this bias. First anneal for several estimated sink times, then perform a fresh short tracer measurement at the same temperature. Agreement of late-time slopes for different initial quench histories supports a common equilibrium diffusion coefficient. Changes in specimen thickness that shorten the distance to a vacancy sink should affect the excess decay stronger than the elementary jump barrier. Verify that changing the thickness has not simultaneously changed grain size or surface diffusion paths. Combining the full time-dependent variance with an independent vacancy-sensitive observable is more informative than treating a series of single final widths as separate equilibria.

Tutorial on activation energies

The slope of $\ln D$ versus $1/T$ is $-1.74 \times 10^{4}\,\mathrm{K}$ in an equilibrated specimen. A short quenched measurement with a fixed vacancy population gives $-5.80 \times 10^{3}\,\mathrm{K}$. Estimate both enthalpies.

▼ **Work through the solution**

Multiplying slopes in magnitude by $k_B = 8.6173 \times 10^{-5}\,\mathrm{eV/K}$ gives approximately $1.50\,\mathrm{eV}$ total and $0.50\,\mathrm{eV}$ migration. Their difference gives $1.00\,\mathrm{eV}$ formation. This inference assumes the same dominant vacancy mechanism and no significant changes of the prefactor or defect population over the quenched measurement.

A tracer profile grows in rms width from 1.5 to $3.0\,\mu\mathrm{m}$ in $3600\,\mathrm{s}$. Estimate the one-dimensional diffusion coefficient.

▼ **Work through the solution**

Subtract the initial variance rather than the initial width:

$$D = [(3.0)^2 - (1.5)^2]10^{-12}/7200 = 9.38 \times 10^{-16}\,\mathrm{m^2/s}.$$

If the instrument resolution changes between runs its variance change must also be estimated. A constant independent resolution cancels in the subtraction.

What would distinguish fast grain-boundary transport from an unexpectedly low bulk migration barrier?

▼ **Work through the solution**

Compare single crystals with specimens of varying grain size at the same thermal history and fit the full profile rather than only its second moment. Enhanced fast tails that grow with boundary area support an additional path. An independent defect-population measurement helps separate a low jump barrier from an enhanced concentration. A single Arrhenius slope represents the dominant observed transport, not a unique proof of its mechanism.

The University of Zurich solid-state course connects microscopic arrangement and macroscopic material response.

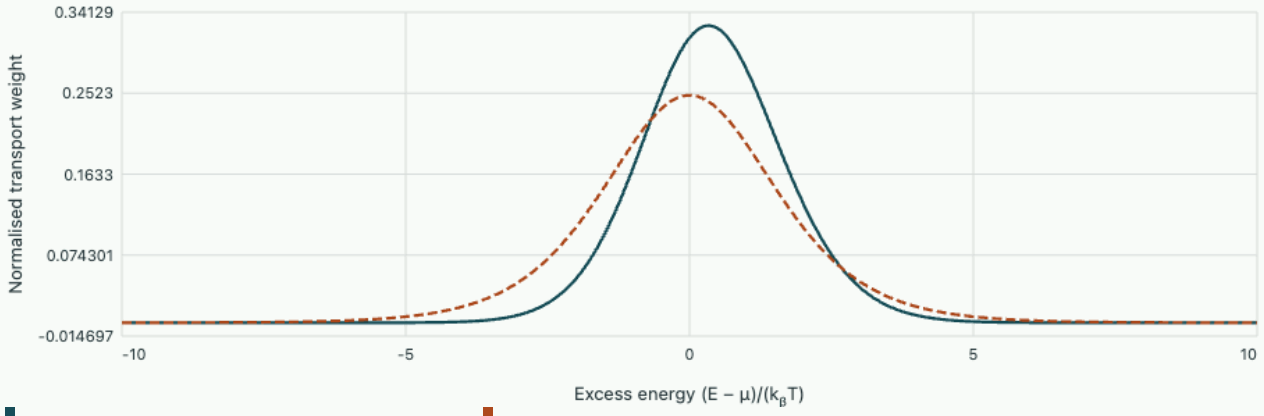
Compare a different inferred transport coefficient with the kinetic factors behind it.

Open this experiment online

Try the calculation

Filter centre $(E - \mu)/(k_\beta T)$ **1**

Filter width / $(k_\beta T)$ **2**



Mean excess energy 0.4018 $k_\beta T$; electron Seebeck coefficient -34.63 µV/K. Open-circuit Lorenz ratio L/L_o = 0.4937.

Structure, excitations and probes of solids · 6. Measure a phonon mean free path without confusing it with a sample length

A cold insulating bar can carry heat primarily through lattice vibrations. Heat capacity tells how much energy the vibrations can carry; conductivity also depends on how far and in which direction they carry it. Derive the connection, test its limiting regimes, and identify when a measured thermal resistance belongs to a boundary.

Derive the kinetic expression from a displaced occupation

Consider phonon modes labelled by wavevector $\mathbf{k}$ and branch s, with angular frequency $\omega_{\mathbf{k}s}$ and group velocity $\mathbf{v}_{\mathbf{k}s} = \nabla_{\mathbf{k}}\omega_{\mathbf{k}s}$. A mode transports energy $\hbar\omega$ per quantum. At equilibrium states with opposite velocities cancel in the heat current. A small slowly varying temperature gradient perturbs the Bose occupation $n_0(T)$. In the relaxation-time approximation the stationary transport equation is

$$\mathbf{v} \cdot \nabla T \, \partial_T n_0 = -\delta n / \tau.$$

This describes weak near-equilibrium transport when a mode can be assigned a characteristic relaxation time.

Insert the correction into the heat current density $\mathbf{j}_Q = V^{-1} \sum \hbar\omega \, \mathbf{v} \, \delta n$. Comparing with $j_{Q,i} = -\kappa_{ij} \partial_j T$ gives

$$\kappa_{ij} = V^{-1} \sum c_{\mathbf{k}s} v_i v_j \tau_{\mathbf{k}s},$$

where $c_{\mathbf{k}s} = \hbar\omega \, \partial_T n_0$ is the heat capacity contribution of one mode. In an isotropic solid the angular average of v_x^2 is $v^2/3$. An effective common speed and path $\ell = v\tau$ then yield $\kappa \simeq C_V v \ell / 3$ for heat capacity per volume C_V. The factor one third counts directional projection, not the three separate phonon branches.

Connect the Debye heat capacity to low-temperature transport

For a three-dimensional isotropic acoustic branch with $\omega = v_s k$, the number of states in a wavevector shell is proportional to $k^2 dk$. Thus its density of states per volume is proportional to ω^2 / v_s^3. In the thermal energy $\int d\omega \, g(\omega) \hbar\omega / (e^{\hbar\omega/k_B T} - 1)$, substitution $x = \hbar\omega / k_B T$ produces a factor T^4 when occupied frequencies remain below the high-frequency cutoff. Differentiation gives

$$C_V \propto T^3.$$

Different sound speeds of longitudinal and transverse branches enter the coefficient. An optical mode with a nonzero minimum frequency contributes much less at sufficiently low temperature.

If rough sample boundaries dominate scattering and give an approximately temperature-independent mean path, the kinetic expression predicts $\kappa \propto T^3$. A more specular boundary can increase the

effective path of long-wavelength modes and modify that exponent. Conversely once many modes are thermally populated, heat capacity tends toward saturation and increasing phonon–phonon or defect scattering can reduce conductivity. Adding rates as $1/\tau = 1/\tau_{\mathrm{b}} + 1/\tau_{\mathrm{defect}} + 1/\tau_{\mathrm{anh}}$ assumes independent effective relaxation mechanisms. Normal phonon collisions conserve crystal momentum and do not always relax heat current as efficiently as a naive single-rate sum implies.

Take an insulating crystal at one temperature with measured $C_V = 40\,\mathrm{J/(m^3K)}$, representative $v = 4000\,\mathrm{m/s}$, and $\kappa = 0.80\,\mathrm{W/(mK)}$. The inferred effective path is $3\kappa/(C_V v) = 15\,\mu\mathrm{m}$, corresponding to $3.75\,\mathrm{ns}$. In a $1.0\,\mathrm{mm}$-wide specimen this is much shorter than its width. An assertion that only diffuse sidewall collisions limit transport would need further evidence. Measuring a second transverse dimension and checking whether the inferred path scales with it is more discriminating than matching a single temperature exponent.

Background · Which temperature does a finite-gradient measurement report?

Suppose the conductivity obeys $\kappa(T) = bT^3$ across a homogeneous bar with a diffusive local temperature field. In a steady state the heat flux is uniform. Integrating Fourier's law shows that dividing the heat flux times length by the end-to-end temperature difference returns the temperature average of κ. Let T_m be the arithmetic mean and $\Delta T = T_h - T_c$.

$$\kappa_{\mathrm{app}} = \frac{1}{\Delta T}\int_{T_c}^{T_h} bT^3\,dT = bT_m^3\left(1 + \frac{\Delta T^2}{4T_m^2}\right).$$

A 1 K drop centred on 2 K raises the apparent conductivity by 6.25% relative to the local value at 2 K. Halving the temperature difference reduces the excess by a factor of four. That dependence gives an experimental check before attributing a deviation to boundary scattering.

Distinguish sample conductivity from contact and ballistic resistance

A steady one-dimensional bar of area A and length L carries power $P = \kappa A \Delta T_{\mathrm{bulk}}/L$ in the diffusive regime. If the two contacts have thermal resistances R_1, R_2, an externally measured temperature difference gives

$$R_{\mathrm{tot}} = \Delta T/P = R_1 + R_2 + L/(\kappa A).$$

A plot of total resistance against length for otherwise equivalent specimens can separate intercept from bulk slope. A contact-limited device fitted as pure bulk appears to have a length-dependent conductivity. At very small lengths, ballistic transport itself supplies a length-independent resistance, which a length sweep alone cannot always distinguish from ordinary contacts.

For area $A = 1.0\,\mathrm{mm}^2$, suppose resistance rises from $3600\,\mathrm{K/W}$ for a $2.0\,\mathrm{mm}$ bar to $8600\,\mathrm{K/W}$ for a $6.0\,\mathrm{mm}$ bar under matched contacts. The slope gives $\kappa = 0.800\,\mathrm{W/(mK)}$ and the intercept

$1100\,\mathrm{K/W}$. At $P = 20\,\mu\mathrm{W}$ the shorter device has an external temperature difference $0.072\,\mathrm{K}$, of which $0.022\,\mathrm{K}$ is attributable to the contacts. Failing to subtract the intercept gives an apparent conductivity only $0.556\,\mathrm{W/(mK)}$. Temperature probes located inside the bar can measure the bulk gradient more directly.

When the path is comparable to a sample dimension the local Fourier relation with one well-defined temperature per point needs justification. In a simple isotropic ballistic picture a reservoir emits an energy flux on one side with angular factor $1/4$, leading to a conductance per area of order $C_V v/4$ for perfectly transmitting contacts. This differs from the $1/3$ in the diffusive expression; the angular integrals describe different boundary-value problems. A finite transmission probability, mode mismatch and partial equilibration near reservoirs can further reduce conductance. A stated mean free path inferred using Fourier's law beyond this crossover is an effective fit, not an independently measured microscopic length.

Estimate when a heater measurement leaves linear response

A cold crystal can have a temperature-dependent conductivity over even a small absolute thermometer difference. In a uniform bar at steady state, constant heat current obeys $PL/A = \int_{T_c}^{T_h} \kappa(T)\,dT$. If $\kappa = \beta T^3$, then $P = \beta A (T_h^4 - T_c^4)/(4L)$. Dividing measured flux by a nominal gradient gives the interval average of conductivity, rather than its exact value at either thermometer temperature. For $T_c = 2\,\mathrm{K}, T_h = 4\,\mathrm{K}$, the averaged conductivity is 30β, whereas κ at the mean temperature $3\,\mathrm{K}$ is 27β. The eleven-percent difference is a consequence of nonlinear temperature dependence, even with perfect contacts and sensors.

Shrink the heater excursion at the same mean temperature to test the small-gradient approximation. A contact bottleneck can itself become nonlinear, in which case subtracting a constant contact resistance found at a different mean temperature is also inappropriate. Modulate a small heating power around a stable bias and analyse the differential thermal resistance, or measure temperatures at internal probes for several heat currents. These protocols probe a particular operating point and can distinguish the curvature of the intrinsic material response from the curvature of the two contact heat-transfer laws.

Tutorial on a thermal measurement

A bar with boundary-limited $C_V \propto T^3$ is cooled from 4 K to 2 K with unchanged diffuse boundary path. How should its thermal conductivity and its diffusivity change?

▼ Work through the solution

Conductivity falls by a factor eight. Thermal diffusivity $\kappa/C_V \simeq v\ell/3$ stays approximately constant. An experiment measuring the relaxation time of a spatial sinusoidal temperature disturbance probes diffusivity, while a steady gradient at given heat flux probes conductivity. The two measurements need not have the same temperature dependence.

Using the worked $15\ \mu\mathrm{m}$ path, predict the thermal diffusivity and the decay time of a long-wavelength sinusoidal temperature modulation with wavelength $1.0\ \mathrm{mm}$.

▼ **Work through the solution**

The diffusivity is

$$0.80/40 = 0.020\ \mathrm{m}^2/\mathrm{s}.$$

The diffusive decay time is

$$1/[D_T(2\pi/\lambda)^2] = 1.27\ \mu\mathrm{s}.$$

Here $k\ell \approx 0.094$, reasonably small. At a wavelength comparable to the inferred path a diffusive exponential should be tested rather than assumed.

A sample's conductivity increases after isotopic purification while its measured heat capacity hardly changes. What microscopic inference is supported?

▼ **Work through the solution**

In the kinetic picture similar heat capacity and sound speed leave a longer weighted phonon path as the natural interpretation. Isotope disorder can scatter vibrations while leaving the gross mode count similar. Check geometric dimensions and contact resistances before attributing the full change to bulk scattering. A mean path deduced this way is weighted by mode heat capacities and velocities, not a single universal length for every phonon.

David Tong counts acoustic and optical phonons and derives their thermodynamics.

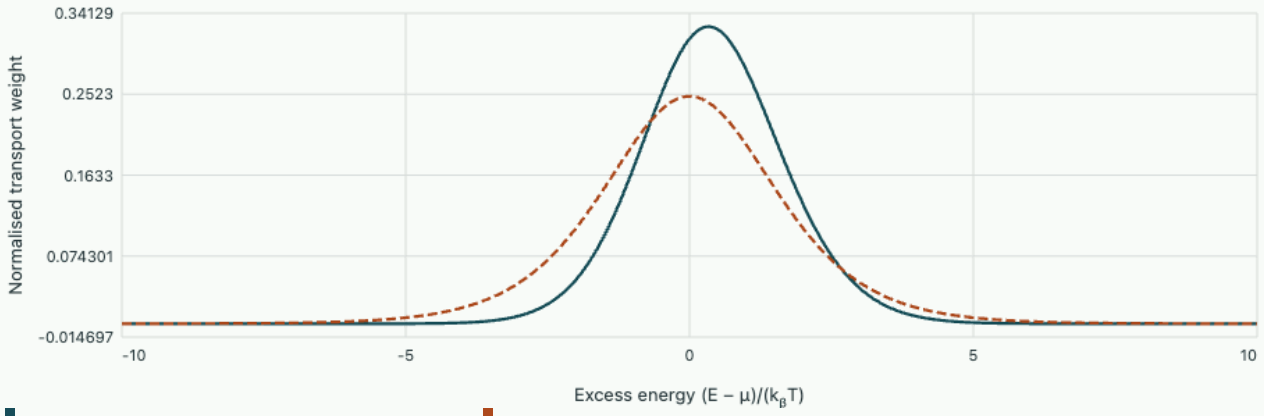
Compare lattice heat flow with heat carried by electronic excitations.

Open this experiment online

Try the calculation

Filter centre $(E - \mu)/(k_\beta T)$ **1**

Filter width / $(k_\beta T)$ **2**



Energy-selected current carriers Smooth metallic transport

Mean excess energy 0.4018 $k_\beta T$; electron Seebeck coefficient -34.63 µV/K. Open-circuit Lorenz ratio $L/L_o = 0.4937$.

Structure, excitations and probes of solids · 7. A field profile that distinguishes a superconductor from a perfect conductor

Zero dc resistance tells how a current can persist. Field expulsion tells how a specimen responds when it enters a superconducting equilibrium state. Derive the London length, calculate what a finite slab and a thin film actually screen, and connect magnetic and electrical measurements to the same superfluid density.

Separate frozen flux from equilibrium screening

For mobile carriers of mass m, charge q and number density n_s, a simple inertial equation $m\dot{\mathbf{v}} = q\mathbf{E}$ gives

$$\partial_t \mathbf{j}_s = n_s q^2 \mathbf{E}/m.$$

This first London equation explains dissipation-free acceleration by an electric field in the ideal response. Take its curl and use Faraday's law: $\partial_t[\nabla \times \mathbf{j}_s + (n_s q^2/m)\mathbf{B}] = 0$ at fixed uniform n_s. The expression in brackets is time independent. This derivative equation by itself allows an arbitrary initial curl–field combination, so it does not force a previously existing static induction to leave a conductor.

In a simply connected, vortex-free equilibrium superconductor the second London relation supplies the missing condition,

$$\nabla \times \mathbf{j}_s = -(n_s q^2/m)\mathbf{B}.$$

A condensate phase argument gives the same curl relation locally: mechanical pair momentum is $\hbar\nabla\varphi - q\mathbf{A}$; on a patch without a vortex $\nabla \times \nabla\varphi = 0$. With $\nabla \times \mathbf{B} = \mu_0 \mathbf{j}_s$ and $\nabla \cdot \mathbf{B} = 0$, take the curl once more to obtain

$$\nabla^2 \mathbf{B} = \mathbf{B}/\lambda_L^2,$$
$$\lambda_L^2 = m/(\mu_0 n_s q^2).$$

The pair of signs yields exponential decay, not sinusoidal oscillation into a bulk specimen.

The effective mass, charge and density must describe the same carriers. For Cooper pairs of mass about $2m_e$, charge magnitude $2e$, and pair density $n_{\text{electron}}/2$, the combination $n_s q^2/m$ agrees with the expression in terms of participating electron density, charge e and mass m_e. Mixing a pair charge with an electron density and electron mass overpredicts the stiffness by a factor of four. A material effective mass or nonlocal response may alter an inferred density, so a penetration-depth measurement fixes the stiffness combination rather than each microscopic parameter separately.

Solve a finite slab in a parallel applied field

A slab fills $-d/2 < x < d/2$ and a uniform applied induction $B_a\hat{z}$ is imposed parallel to both faces. Assume the Meissner regime, negligible demagnetising fields, and a thickness large compared with microscopic dimensions needed for continuum electrodynamics. The even London solution is

$$B_z(x) = B_a \cosh(x/\lambda_L)/\cosh[d/(2\lambda_L)].$$

Its current is $j_y = -(1/\mu_0)\partial_x B_z$, of opposite signs on the two faces. The mean induction is

$$\frac{\bar{B}}{B_a} = \frac{2\lambda_L}{d}\tanh\frac{d}{2\lambda_L}.$$

In a thick slab the centre field is exponentially small while the average falls only as $2\lambda_L/d$, because a surface layer from each face still contains field. A probe at the centre and one measuring total flux through the cross section thus report different thickness dependence. In a thin slab the average is $1 - d^2/(12\lambda_L^2) + \cdots$, giving weak screening of a parallel field. This is not the perpendicular-field screening problem for a thin film, where fields outside the sample and lateral geometry lead to another length scale.

For $\lambda_L = 100\,\mathrm{nm}$, $d = 400\,\mathrm{nm}$, the centre ratio is $\operatorname{sech} 2 = 0.266$ and the mean ratio is

$$\tanh 2/2 = 0.482.$$

With $B_a = 0.50\,\mathrm{mT}$ the current magnitude just inside a face is

$$B_a \tanh 2/(\mu_0\lambda_L) = 3.84 \times 10^9\ \mathrm{A/m^2}.$$

It flows only over a thin scale. If a material's critical current or critical field is exceeded, this linear vortex-free solution ceases to describe the experiment. Driven hysteresis or trapped vortices can then make the same external field produce different internal profiles after different preparation histories.

Connect kinetic energy to a sheet inductance

A thin uniform strip of length l, width w, thickness $d \ll \lambda_L$ carries a current nearly uniformly through its thickness in a suitable transport geometry. The carrier kinetic energy per volume is

$$mn_s v^2/2 = mj_s^2/(2n_s q^2) = \mu_0\lambda_L^2 j_s^2/2.$$

Integrating over volume and using $j_s = I/(wd)$ gives $E_{\mathrm{kin}} = L_k I^2/2$ with $L_k = \mu_0\lambda_L^2 l/(wd)$. Thus the sheet kinetic inductance is $L_{k,\square} = \mu_0\lambda_L^2/d$, and the number of squares is l/w. It is distinct from geometric inductance storing energy in the magnetic field around the wire.

For $d = 20\,\mathrm{nm}$, $\lambda_L = 100\,\mathrm{nm}$ the sheet value is about $0.628\,\mathrm{pH}$ per square. A strip containing two thousand squares gives $1.26\,\mathrm{nH}$ of kinetic inductance. Its resonance with a capacitor probes the sum

of this inductance and geometric or stray contributions. If the superfluid density falls while the effective mass stays approximately fixed, λ_L^2 increases and the resonant frequency tends to decrease. Measuring several lengths and widths can distinguish a distributed kinetic contribution from an approximately constant lead contribution. At frequencies approaching the gap scale a purely nondissipative London description is insufficient.

Determine what a thickness series can identify

A thin-film measurement sometimes fits the sheet kinetic inductance at a single thickness and quotes a bulk condensate density. In the uniform-film limit the measured product is $L_{k,\square} d = \mu_0 \lambda_L^2$. A thickness calibration error therefore rescales the inferred stiffness even if the resonance frequency is measured extremely accurately. For the $20\,\mathrm{nm}$ example, a systematically inactive layer of $2.0\,\mathrm{nm}$ leaves only $18\,\mathrm{nm}$ contributing. Substituting the nominal thickness into a stiffness inference underestimates the conducting carrier density by ten percent if the other model assumptions hold. A series of films and an independent estimate of the active thickness can test this interpretation.

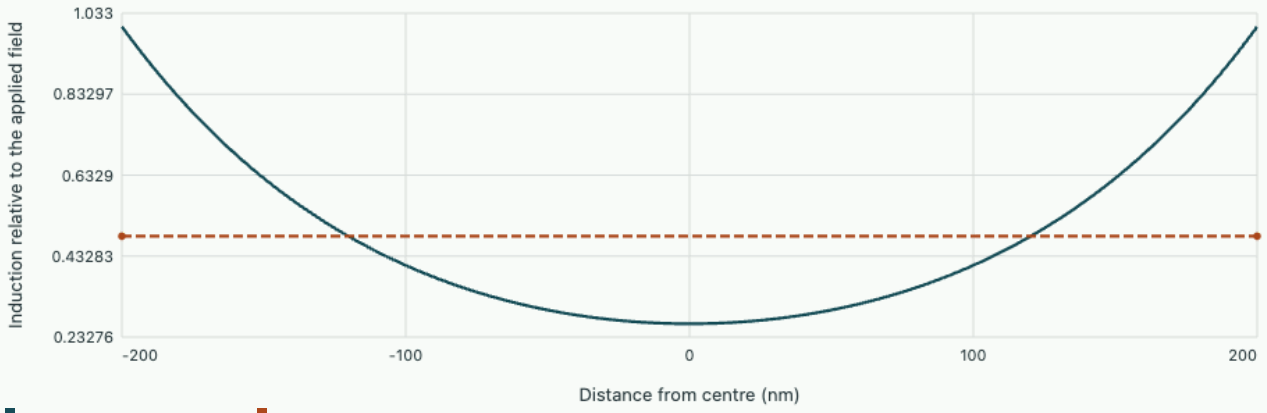
Compare with the parallel-field slab calculation by changing the ratio of thickness to penetration depth in the live profile. At a ratio of one, the centre and surface inductions differ only modestly. At a ratio of ten the interior is nearly field free while a substantial fraction of the averaged flux still resides near the two faces. The programme graphs B/B_a across the physical thickness and reports both centre and mean, which are different experimental weightings of the same field. Compare those numbers with an independently measured kinetic inductance before attributing a temperature shift entirely to an altered carrier density. Higher kinetic inductance can also reflect an increased effective mass or a reduced active cross section.

Open this experiment online

Try the calculation

Film thickness (nm) **400**

London length (nm) **100**



Local induction Cross-section mean

At the centre B/Ba = 0.2658, whereas the cross-section mean is 0.4820. These apply to a parallel field in a vortex-free slab.

Compare parallel screening with a perpendicular-field measurement

For a wide film in perpendicular field the magnetic flux lines bend around the edges, and the one-dimensional parallel-field cosh solution no longer applies. Sample width, aspect ratio and the field outside the superconducting material enter the response. Rotate the same thin film through ninety degrees and an apparent change in susceptibility may therefore be largely geometrical. Verify orientation and demagnetising conditions before combining the two datasets into one estimate of penetration depth.

Tutorial on comparing probes

A thick slab shows a centre field less than one percent of the applied parallel field. What lower bound on d/λ_L follows from the local London solution?

▼ **Work through the solution**

Require $\cosh[d/(2\lambda_L)] > 100$, hence $d/\lambda_L > 2\,\mathrm{arcosh}(100) \approx 10.60$. The mean field at this threshold would still be about $2/10.60 = 0.189$ of the applied field. A centre measurement at one percent therefore does not imply a one-percent cross-section average.

If the superfluid charge stiffness $n_s q^2/m$ falls by half, how do penetration depth and sheet kinetic inductance change for the same film?

▼ **Work through the solution**

The penetration depth increases by $\sqrt{2}$, and the sheet kinetic inductance doubles because it scales as λ_L^2. A resonance in which kinetic inductance is only one quarter of total inductance will shift less than the $1/\sqrt{2}$ expected if all inductance doubled. The initial circuit partition must be estimated.

A ring retains flux after cooling in a field. Does this disprove the equilibrium slab result?

▼ **Work through the solution**

The slab derivation assumed simple connectivity, a vortex-free state and prescribed fields on two faces. A ring permits nontrivial phase winding and fluxoid quantisation. A multiply connected circuit can maintain trapped flux even with local London screening in its material. Compare with a simply connected specimen under controlled zero-field cooling and field-cooling protocols before interpreting the ring as a direct slab test.

The University of Zurich solid-state course includes superconductivity and its magnetic signatures.

Compare ordinary resistive field diffusion with an equilibrium London profile.

Structure, excitations and probes of solids · 8. Infer a superconducting gap from a tunnelling spectrum

A tunnel junction reports differential conductance versus voltage. Extracting a superconducting energy gap requires connecting a condensate's quasiparticle dispersion to a density of states, then accounting for temperature and finite spectral resolution before comparing peaks with the data.

Diagonalise the paired-state Hamiltonian

In a simple isotropic weak-coupling description, pair a state of normal-state energy $\xi_k = \epsilon_k - \mu$ with the time-reversed hole amplitude. Take a real gap $\Delta > 0$ by a phase choice. The two-component mean-field matrix has rows (ξ_k, Δ) and $(\Delta, -\xi_k)$, giving eigenvalues $\pm E_k$ with $E_k = \sqrt{\xi_k^2 + \Delta^2}$. The positive-energy quasiparticle mixes particle-like and hole-like amplitudes with squared coefficients $(1 + \xi_k/E_k)/2$ and $(1 - \xi_k/E_k)/2$. Their sum is one. Near the normal-state Fermi surface they are equal, while far above it the excitation becomes predominantly particle like.

The minimum positive excitation energy is Δ. Creating two independent quasiparticles requires at least 2Δ in the ideal isotropic spectrum. These two thresholds refer to different probes. In an ideal normal-metal–insulator–superconductor tunnel junction, a bias can transfer one electron into an allowed quasiparticle state; the zero-temperature threshold is $|eV| = \Delta$. In a junction between two identical gapped electrodes, lowest-order quasiparticle tunnelling at zero temperature instead begins near 2Δ, aside from pair tunnelling and other processes. Confusing the physical junction type can double the reported gap.

Transform the normal-state density of levels

Assume approximately constant normal electronic density near the Fermi level over an energy range much larger than Δ. The quasiparticle dispersion flattens near $\xi = 0$. Mapping the two normal-state branches $\xi = \pm\sqrt{E^2 - \Delta^2}$ onto a positive energy and accounting for their electron spectral weights gives the normalised superconducting tunnelling density

$$\frac{N_s(E)}{N_n(0)} = \begin{cases} 0, & |E| < \Delta, \\ |E|/\sqrt{E^2 - \Delta^2}, & |E| > \Delta. \end{cases}$$

The divergence at the gap edge is integrable. Indeed integrating from Δ to $A > \Delta$ gives $\sqrt{A^2 - \Delta^2}$, tending toward the corresponding normal integral at large cutoff. The edge feature represents redistribution of states from the gap, rather than creation of an infinite number of states. In a finite normal band the constant-density approximation is only local, so statements about total spectral weight should use a consistent large-energy model.

For $\Delta = 1.50\,\mathrm{meV}$, the ideal density at $E = 2.00\,\mathrm{meV}$ is $2/\sqrt{4 - 2.25} = 1.51$ times the normal level. At $5.0\,\mathrm{meV}$ it is approximately 1.048, illustrating the slow approach to the normal baseline. A normalising window too close to the edge can bias the whole inferred curve downward. A comparison with a normal-state spectrum taken with the same junction can control a varying normal density or voltage-dependent transmission better than a single distant conductance point.

Derive the thermal convolution measured by a normal probe

In lowest-order tunnelling with a featureless normal tip and approximately constant matrix elements, the current is proportional to $\int N_s(E)[f(E-eV)-f(E)]\,dE$. The two Fermi factors count occupied initial and available final states. Differentiating in bias gives normalised conductance $G(V)/G_n = \int [N_s(E)/N_n][-f'(E-eV)]\,dE$. Here $-f'(x) = \operatorname{sech}^2[x/(2k_BT)]/(4k_BT)$ has unit integral. At zero temperature it becomes a delta function and the conductance reproduces the density. At finite temperature it samples a window: conductance can be nonzero inside the underlying hard gap without any actual subgap states.

The full width at half height of this derivative is $4k_BT\,\operatorname{arcosh}\sqrt{2} \approx 3.53k_BT$. At $T = 2.0\,\mathrm{K}$ this is $0.608\,\mathrm{meV}$, appreciable compared with a $1.50\,\mathrm{meV}$ gap. The electron temperature at the tunnel contact can exceed the temperature reading of a nearby bath. Voltage noise and a finite lock-in excitation add other convolution kernels. A fit that varies gap, thermal width and lifetime broadening all freely against a single narrow window can have strongly correlated parameters. Measure an independent thermal reference or repeat with deliberately varied excitation to separate instrumental from material broadening.

Compute the ideal convolution with an edge-safe quadrature

Numerically sampling the divergent density at one grid point exactly on the edge gives an artificial infinity. A variable transformation removes it. For $E > \Delta$ set $\xi = \sqrt{E^2-\Delta^2}$. Then $(E/\sqrt{E^2-\Delta^2})\,dE = d\xi$. Integrate over positive ξ and include the negative-energy mirror:

$$G/G_n = \int_0^\infty [K_T(\sqrt{\xi^2+\Delta^2}-eV) + K_T(-\sqrt{\xi^2+\Delta^2}-eV)]\,d\xi.$$

Both terms are smooth at zero for positive temperature. This numerical reformulation follows directly from state counting.

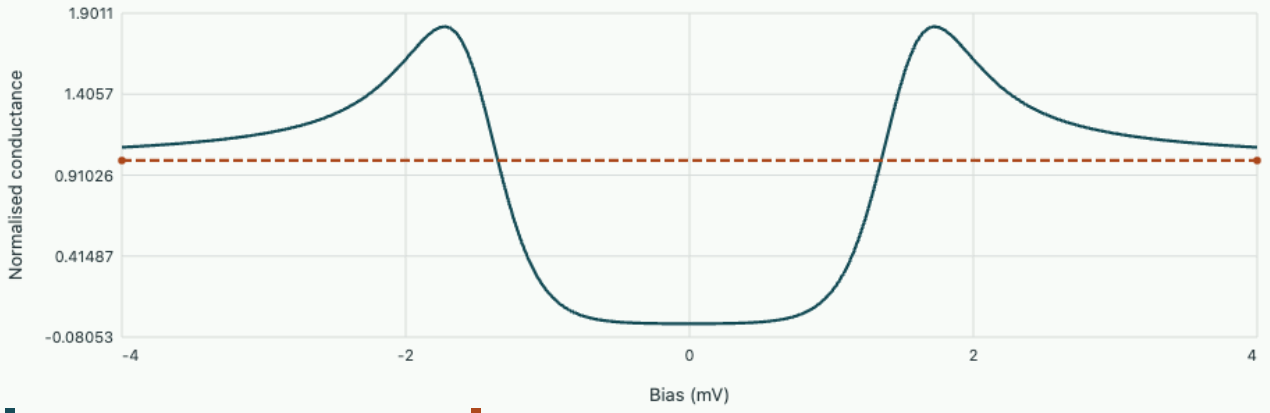
The live spectrum uses this transformed integral with energies in meV and voltages in mV for a single electron. First choose a low but finite temperature and locate the two coherence features. Increase temperature at fixed Δ to isolate the effect of the measurement kernel. A physically heated sample would generally also have a temperature-dependent gap; this controlled calculation keeps the intrinsic spectrum explicit. Compare the zero-bias conductance, peak height and high-bias baseline. A change in one feature alone seldom establishes the source of broadening.

Open this experiment online

Try the calculation

Gap Δ (meV) **1.5**

Electron temperature (K) **2**



Thermally broadened tunnelling Normal-state reference

Thermal kernel FWHM 0.608 meV. Zero-bias conductance is 0.0013 of the normal value. Gap and probe temperature vary independently.

Identify a spectral asymmetry that the symmetric model cannot fit

For a featureless normal tip and a particle–hole symmetric superconducting spectrum, the convolution with the even thermal kernel gives

$$G(V) = G(-V).$$

The average of opposite bias measurements estimates the even component, while half their difference isolates an odd component. A small bias-offset calibration error V_0 produces an apparent odd part approximately $-V_0\, dG_{\mathrm{even}}/dV$ for small shifts. It is therefore largest on steep gap-edge flanks and changes sign when the bias offset reverses. An energy-dependent normal background can generate a smoother intrinsic asymmetry; a temperature sweep through the transition and an independent voltage-zero calibration help distinguish these mechanisms.

Suppose the spectral flanks have slope $1.8 G_n/\mathrm{mV}$ and the measured odd part peaks near $0.036 G_n$. A voltage offset of only $0.020\,\mathrm{mV}$ could generate that size, much smaller than the illustrative gap. Comparing the sign pattern on both flanks tests the derivative shape rather than fitting one data point. A single shifted peak position can reflect offset, thermal broadening or changing gap amplitude. Record both bias directions, both coherence peaks and their separation as well as their midpoint. A common shift of both peaks changes the midpoint but ideally leaves their separation unchanged.

The model also assumes a normal electrode with roughly flat density. If the tip itself is superconducting, the current is a convolution of both electrode densities and their occupation

difference. In that case symmetric features can shift even when the sample gap is unchanged, requiring an independent tip calibration or a different junction model.

Tutorial on tunnelling data

An ideal normal-tip spectrum at very low temperature has gap edges separated by $3.20\,\mathrm{mV}$. Estimate Δ, and compare with a weak-coupling transition temperature using $2\Delta/(k_B T_c) \approx 3.53$.

▼ **Work through the solution**

The symmetric single-particle edges lie near $\pm\Delta/e$, hence $\Delta \approx 1.60\,\mathrm{meV}$. Inserting $k_B = 0.08617\,\mathrm{meV/K}$ gives $T_c \approx 10.5\,\mathrm{K}$. This ratio is a weak-coupling benchmark for the isotropic model, not an exact conversion for every material. Verify the actual transition and junction type independently.

An experiment at $4.2\,\mathrm{K}$ tries to distinguish two gaps differing by $0.10\,\mathrm{meV}$ using peak positions alone. Which scale should be compared first?

▼ **Work through the solution**

The thermal derivative width is $3.53(0.08617)(4.2) \approx 1.28\,\mathrm{meV}$, much larger than that gap difference. High signal quality and a constrained model can sometimes infer parameters finer than a raw linewidth, but separate visible peaks are unlikely from thermal resolution alone. Lower electron temperature and calibrated voltage modulation add stronger discriminating evidence.

What check distinguishes a quadrature error from true thermal subgap conductance?

▼ **Work through the solution**

Refine the transformed integration grid, extend its energy cutoff and confirm the conductance is even in voltage for this symmetric model. A normal reference with $\Delta = 0$ should yield unity at every bias when the kernel is fully integrated. The computed zero-bias value for positive gap should fall as temperature decreases. A subgap signal sensitive to whether an energy grid happens to land on an edge is a numerical artifact.

The University of Zurich solid-state course develops superconducting excitations and their physical consequences.

Structure, excitations and probes of solids · 9. Read twist and mismatch from the moiré of two lattices

Stack two square grids that differ slightly in orientation or pitch. The slowly varying registry map is visible over many unit cells. Derive its scale and direction in reciprocal space, and find which combinations of layer parameters a single period measurement can resolve.

Subtract two spatial phases

One family of planes in layer one carries a density modulation proportional to $\cos(\mathbf{G}_1 \cdot \mathbf{r})$, with $|\mathbf{G}_1| = 2\pi/a$. Layer two has spacing $a(1+\delta)$ and is rotated by θ. Multiplying their modulations, as in a local registry correlation, produces half the sum of two cosines. The rapidly varying term contains $\mathbf{G}_1 + \mathbf{G}_2$; averaging over several original cells leaves the term with $\Delta\mathbf{G} = \mathbf{G}_1 - \mathbf{G}_2$. A distance parallel to $\Delta\mathbf{G}$ that advances the resulting phase by 2π spans one full registry period.

Taking the dot product of the rotated reciprocal vectors gives the exact geometric scale

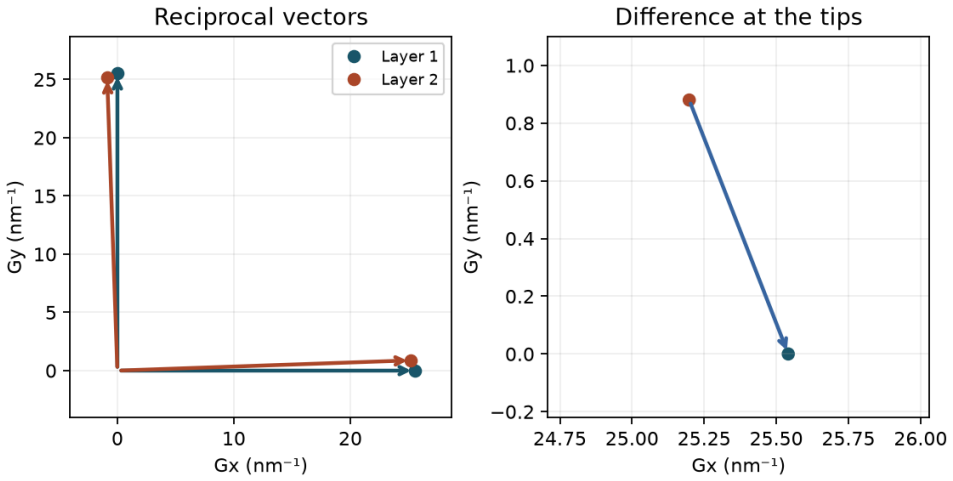
$$\frac{\Lambda}{a} = \left[1 + \frac{1}{(1+\delta)^2} - \frac{2\cos\theta}{1+\delta}\right]^{-1/2}.$$

The second perpendicular family of a square lattice rotates and rescales the same way. Its difference vector is perpendicular to the first and has the same magnitude. Their two slow cosines generate a square registry pattern. For small mismatch and small twist measured in radians the period is approximately $a/\sqrt{\delta^2+\theta^2}$. The interference construction specifies a local continuum period. An exact common atomistic supercell would require additional commensurability conditions.

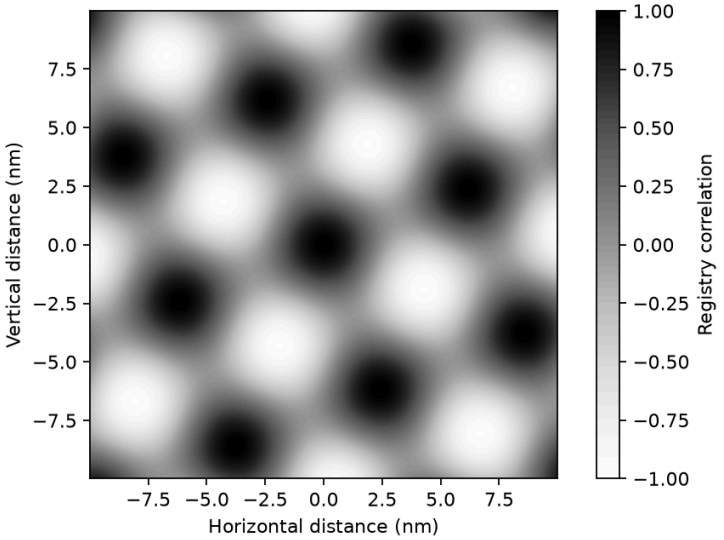
Interpret a long measured period

Take $a = 0.246$ nm, mismatch 1.3 percent and twist two degrees. In units of $2\pi/a$ the horizontal family's difference vector is $(1-\cos\theta/(1+\delta), -\sin\theta/(1+\delta))$, approximately $(0.0134, -0.0345)$. Its length is about 0.0370, so the registry period reaches about 6.65 nm. Each layer still has a spacing near a quarter nanometre. The larger scale is the distance over which small phase differences accumulate.

If an image measures only this period and the first layer spacing, it supplies a single scalar for the two unknowns δ and θ. A reciprocal-space measurement referenced to the first lattice supplies direction as well. In the simple isotropic model this resolves the rotated and rescaled vector by $\mathbf{G}_2 = \mathbf{G}_1 - \Delta\mathbf{G}$. Additional distortions or strain require more directions before an inversion is possible.



The right panel enlarges the displacement between reciprocal-vector tips. Its direction is the normal to one family of registry fringes.



The map sums the two perpendicular slow modulations; the colour bar measures their dimensionless average. At perfect alignment with equal spacing the registry is constant everywhere.

Exercise · determine a twist from pure rotation

The lattice spacings have been verified equal at 0.246 nm. What is the magnitude of the twist if the registry spacing is 10.0 nm?

▼ Work through the solution

With $\delta = 0$, the reciprocal vectors form an isosceles triangle and $\Lambda = a/[2|\sin(\theta/2)|]$. The small positive solution is $2\arcsin(0.246/20.0) = 0.02460$ rad or 1.41 degrees. Changing the twist sign reflects the pattern without changing its period.

Exercise · make the same spacing with no twist

Use the same first-layer spacing and measured 10.0 nm period. What positive mismatch would explain the observation for aligned layers?

▼ **Work through the solution**

At $\theta = 0$ and positive mismatch,

$$\Lambda = a(1+\delta)/\delta.$$

Solving gives $\delta = a/(\Lambda - a) = 0.02522$, about 2.52 percent. Comparing this result with the previous exercise shows explicitly why period alone cannot identify a twist.

Try it · Moire

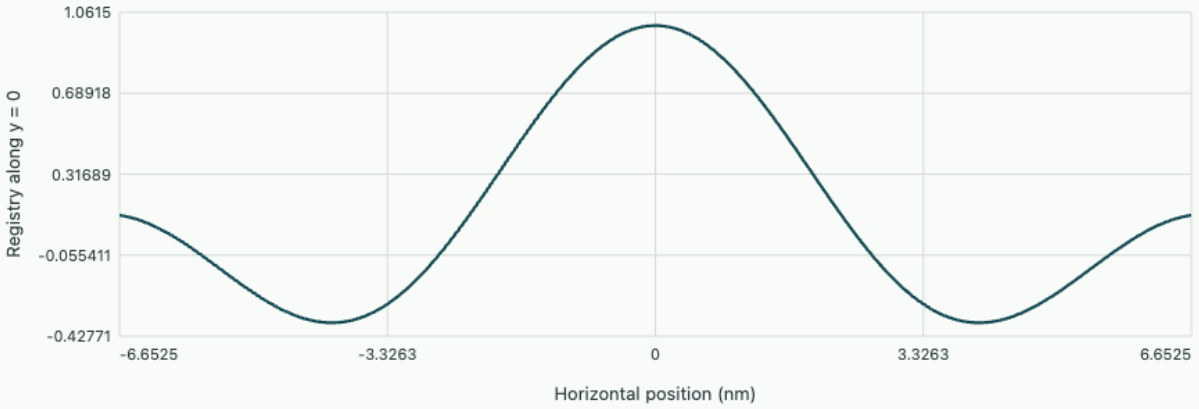
Change the inputs and compare the recalculated curves with the preceding derivation and baseline figure. The axes give the units; the numerical readout states the models assumptions and any limiting cases. Reset the inputs to return to the reference setting.

Open this live calculation

Try the calculation

Lattice mismatch **0.013**

Relative twist (degrees) **2**



Two perpendicular registry modulations

Registry period 6.6525 nm; reciprocal mismatch magnitude 0.94448 nm⁻¹.

Download the corresponding editable notebook. The browser recalculates the reduced equations directly; the notebook exposes the full calculation and its checks.

Open editable notebook

Download .ipynb

Structure, excitations and probes of solids · 10. From bonding energy to lattice spacing and sound speeds

Diffraction gives a spacing and ultrasound gives a stiffness. One measures where an energy curve is stationary, the other measures its curvature. Building the simplest energy of an ionic solid gives both observables and shows which quantities a spring model has already assumed.

Decide which degrees of freedom contribute to binding

In an ionic crystal the leading energy is the electrostatic interaction of charged sublattices. In a covalent solid electron sharing favours specific bond directions, as in a tetrahedrally coordinated network. In a metal the mobile electronic states extend across the lattice and contribute an energy that depends on occupation and interatomic spacing. Closed-shell atoms can attract through fluctuating dipoles even when they have no permanent dipole. At small separations overlapping electronic clouds incur a rapidly rising energy. These mechanisms can coexist. No single pair potential reproduces every elastic or optical property.

For an alternating line of charges separated by r, the electrostatic potential at a positive ion receives two contributions at each distance jr. Summing nearest positive and negative shells in neutral groups gives the dimensionless lattice sum $2(1-1/2+1/3-\cdots)=2\ln 2$. In three dimensions the corresponding Madelung constant depends on structure. Neutral summation or a convergent Ewald construction is needed for a Coulomb lattice. A naive rapidly growing box of uncompensated charges can give a spurious result.

Find the energy minimum and infer the short-range repulsion

For one formula unit of a 1:1 ionic lattice take $\Phi(r)=-A/r+B/r^{n}$ with $A=\alpha e^{2}/(4\pi\epsilon_{0})$ and $n>1$. Counting pair energy once gives this coefficient per monovalent ion pair. The stationarity condition at measured nearest-neighbour spacing r_{0} eliminates B. The cohesion and curvature at the same point become

$$B=\frac{Ar_{0}^{n-1}}{n},$$

$$\Phi(r_{0})=-\frac{A}{r_{0}}\left(1-\frac{1}{n}\right),$$

$$\Phi''(r_{0})=\frac{(n-1)A}{r_{0}^{3}}.$$

The energy zero here is separated ions. Getting the cohesive energy relative to separated neutral atoms additionally requires the ionisation and electron-affinity terms. For a rock-salt structure $\alpha=1.7476$ and the volume per formula unit is $v=2r^{3}$. At zero pressure $K=v\,d^{2}\Phi/dv^{2}=v\Phi''/(dv/dr)^{2}$. Substitution gives

$$K=\frac{\Phi''(r_{0})}{18r_{0}}=\frac{(n-1)A}{18r_{0}^{4}}.$$

For $r_0 = 0.282$ nm, $n = 9$ and $e^2/(4\pi\epsilon_0) = 1.440$ eV nm, the model gives $A = 2.517$ eV nm, binding relative to separated ions of 7.93 eV per pair, and $K \simeq 28.3$ GPa. Inverting the curvature using an independently measured modulus tests the assumed repulsive exponent.

Recall · Radial curvature and a bulk modulus have different units

The curvature of one pair energy has units N/m. An elastic modulus has units N/m² and refers to energy per volume. The volume per formula unit and the density of bonds determine the conversion.

Resolve the stiffness tensor using three acoustic polarisations

For a crystal write $\sigma_{ij} = C_{ijkl}\varepsilon_{kl}$. Substitute a displacement $\mathbf{u} = \mathbf{e}\, e^{i(k\mathbf{n}\cdot\mathbf{x}-\omega t)}$ into $\rho\ddot{u}_i = \partial_j\sigma_{ij}$. The strain symmetry gives a symmetric three-dimensional eigenproblem. Its eigenvectors give mode polarisations and its eigenvalues give measurable phase speeds.

$$\Gamma_{ik}e_k = \rho c^2 e_i,$$
$$\Gamma_{ik} = C_{ijkl}n_j n_l.$$

Cubic symmetry leaves C_{11}, C_{12}, C_{44}. Along [100] the eigenvalues are C_{11}, C_{44}, C_{44}. Along [110] they are $(C_{11}+C_{12}+2C_{44})/2$, $(C_{11}-C_{12})/2$, and C_{44}. Under hydrostatic load $K = (C_{11}+2C_{12})/3$. A bulk modulus from ionic compression supplies just one combination. Shear-wave data probe independent curvature directions.

OneSimulation experiment · Three acoustic branches in a cubic crystal

Try a three-dimensional acoustic-speed surface

Rotate the 3D surface to compare propagation along an edge, a face diagonal and a body diagonal. Its radius in a direction is the selected phase speed in that direction. The 2D plot shows the three sorted eigenvalues in the (001) plane; the branch selector changes which one is drawn in 3D.

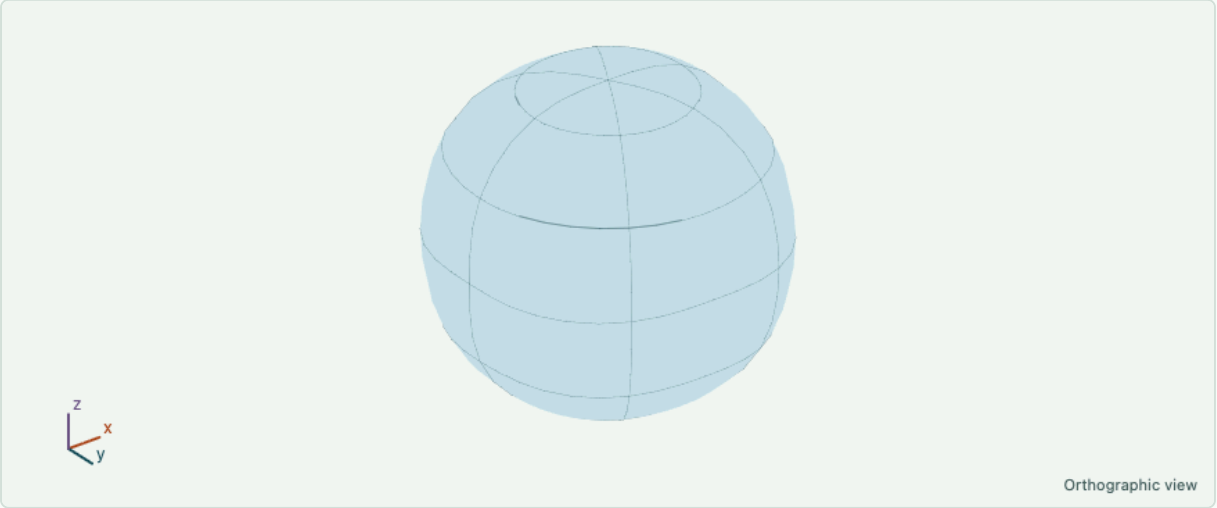
Set C44 to 51 GPa to satisfy C11 – C12 = 2C44. Predict the shape of the surface before moving the slider. Then multiply density by four and check the predicted factor of two in speed. C11 = 166 GPa and C12 = 64 GPa stay fixed. Every surface point solves the symmetric 3 × 3 Christoffel eigenproblem with a browser Jacobi iteration. The full-direction notebook below independently computes the entire surface with OneSimulation, including its [100], [110] and [111] cuts and an isotropic-limit check.

The surface gives phase velocity. In an anisotropic crystal the energy-flow direction can differ from the wave-normal direction, so this surface is not a point-source wavefront.

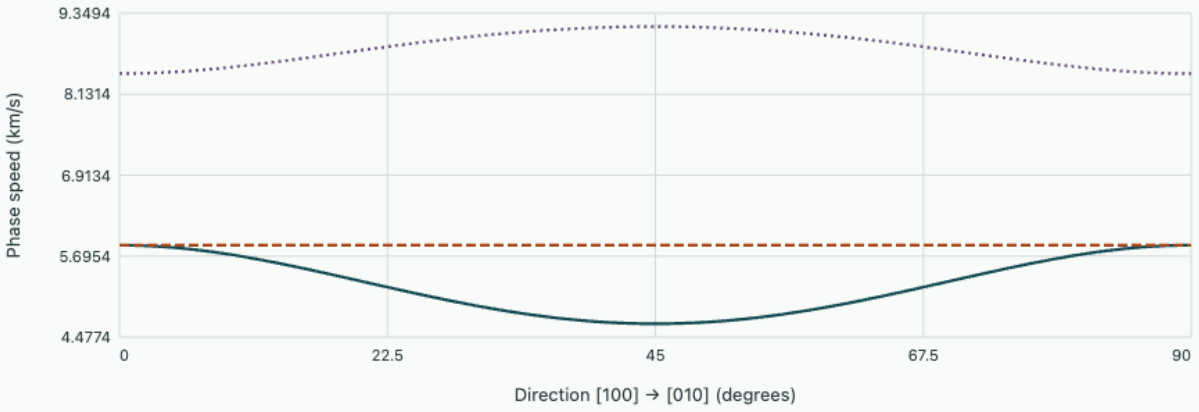
Open this experiment online

Try the calculation

Shear stiffness C44 (GPa)	**80**
Density (kg/m³)	**2330**
3D branch: 0 slow, 1 middle, 2 fast	**2**



Three-dimensional phase-speed surface: in each propagation direction n, the radius is the selected eigenvalue's speed v(n). Coordinates are v(n)n in km/s. This is a material property surface, not a deformed crystal or a group-velocity wavefront. Axes: x = vx (km/s); y = vy (km/s); z = vz (km/s).



Slow branch | Middle branch | Fast branch

C11 = 166 GPa, C12 = 64 GPa. [100] speeds: 5.85959, 5.85959, 8.44065 km/s; [110]: 4.67851, 5.85959, 9.14828 km/s. C44 = 51 GPa makes the material isotropic. The 3D view shows the fast branch.

Download the OneSimulation model

In your OneSimulation environment, run the model with these inputs.

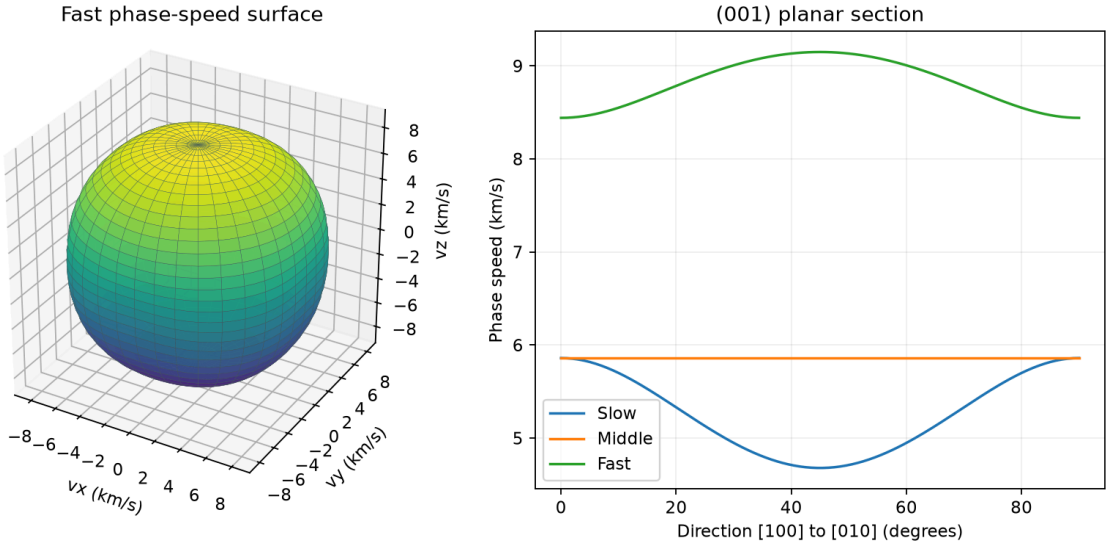
```
python complete-physics-cubic-surface.py --c44 80 --density 2330 --
branch 2
```

Full three-dimensional OneSimulation result

Download the executed 3D notebook · Download the parameterised 3D script. The script command above follows all three controls. Every surface vertex solves the Christoffel eigenproblem in its own propagation direction.

```
from onesim.numerics.linear.matrices.dense_linear_algebra import symmetric_eigenvalues
# n is a unit propagation direction; stiffnesses are in GPa.
gamma = (64. + c44) * np.outer(n, n)
gamma += np.diag(c44 + (102. - 2*c44) * n**2)
velocity = np.sqrt(symmetric_eigenvalues(gamma) * 1e9 / density) / 1000
surface_point = velocity[branch] * n
```

```
[100] 5.859587 5.859587 8.440654 km/s
[110] 4.678505 5.859587 9.148278 km/s
[111] 5.102666 5.102666 9.372287 km/s
Isotropic directional invariance: verified
```



Executed OneSimulation output for C44=80 GPa and density 2330 kg/m³. The surface samples all polar and azimuthal directions; the planar curves provide a reproducible section through it.

Reproduce with OneSimulation

Rotate the propagation direction without changing density or stiffness. Predict which two modes coincide along a cube edge and compare the computed [110] speeds with the three analytic eigenvalues. Then impose the isotropic condition.

Run the downloaded notebook with OneSimulation, NumPy and Matplotlib installed. The output below was recorded with the displayed calculation.

```
"""Sound velocities when a wave rotates through the (001) plane of a cubic solid."""
import numpy as np
import matplotlib.pyplot as plt
from onesim.numerics.linear.matrices.dense_linear_algebra import symmetric_eigenvalues

c11, c12, c44 = np.array([166, 64, 80]) * 1e9  # Pa
```

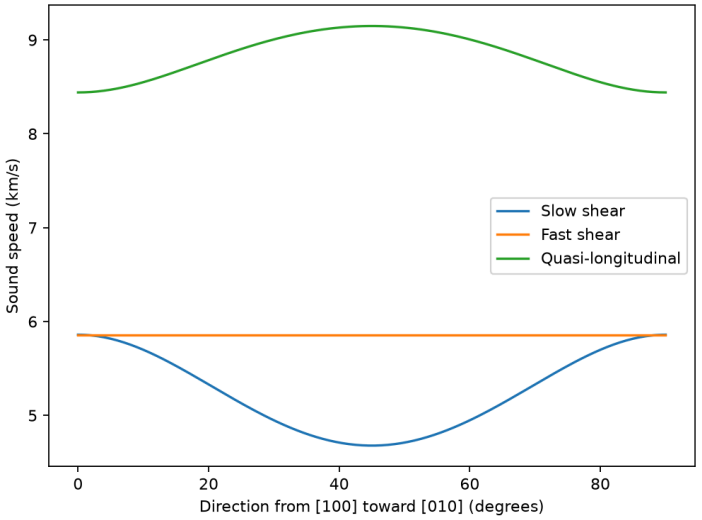
```
density = 2330.0  # kg/m^3

def speeds(angle):
    n = np.array([np.cos(angle), np.sin(angle), 0])
    gamma = (c12+c44) * np.outer(n, n)
    gamma += np.diag(c44 + (c11-c12-2*c44)*n**2)
    return np.sqrt(symmetric_eigenvalues(gamma)/density)

angle = np.linspace(0, np.pi/2, 181)
velocity = np.array([speeds(a) for a in angle]) / 1000
print("Wave speeds in km/s, sorted by magnitude")
for label, a in [("[100]", 0), ("[110]", np.pi/4)]:
    print(label, " ".join(f"{v/1000:.3f}" for v in speeds(a)))
for branch, label in enumerate(["Slow shear", "Fast shear", "Quasi-longitudinal"]):
    plt.plot(np.degrees(angle), velocity[:,branch], label=label)
plt.xlabel("Direction from [100] toward [010] (degrees)")
plt.ylabel("Sound speed (km/s)")
plt.legend()
plt.tight_layout()
plt.savefig("physics-cubic-sound.png", dpi=160)
```

Computed output

```
Wave speeds in km/s, sorted by magnitude
[100] 5.860 5.860 8.441
[110] 4.679 5.860 9.148
```



Three acoustic branches in a cubic crystal.

Download editable notebook · Download Python script

Tutorial on identifying a binding law

1 · Recognise a false equilibrium

▼ **Work through the solution**

With only $-A/r$ the energy falls monotonically as ions approach. A measured lattice spacing and a real sound speed require an energy minimum with positive curvature. Attraction alone supplies neither.

---

2 · Recover one modulus from a transverse mode

▼ **Work through the solution**

At density 2330 kg/m³ an out-of-plane shear mode along [110] travels at 5.86 km/s. Hence $C_{44} = \rho c^2 \simeq 80.0$ GPa. The slower in-plane shear mode instead measures $(C_{11} - C_{12})/2$.

---

3 · Decide whether an isotropic model could fit both shear waves

▼ **Work through the solution**

Cubic shear degeneracy for all directions requires $C_{11} - C_{12} = 2C_{44}$. The notebook uses 102 versus 160 GPa, so a scalar shear modulus cannot fit both [110] speeds. Alter C_{44} to 51 GPa and predict the angular plot before rerunning.

For further study see Kittel, Introduction to Solid State Physics, 8th edition, chapters 1–5 on crystal structure, binding, elastic constants and acoustic lattice modes.

Structure, excitations and probes of solids · 11. Collective charge oscillations, bound excitons and lattice-dressed electrons

A loss peak in an electron spectrum, a line below an optical gap and an enhanced carrier mass call for different kinds of excitations. Start each model with its moving charges and its restoring interaction. That identifies what a measurement can determine.

Displace an electron fluid against its background

Consider a wide slab with carrier number density n, band mass m^* and immobile neutralising positive background. Displace the electron cloud uniformly through a small distance u normal to the faces. The opposite surface charges have magnitude neu per area and generate a restoring field $E = neu/(\epsilon_0\epsilon_\infty)$ inside. The factor ϵ_∞ accounts for faster electronic degrees of freedom excluded from the carrier model.

$$m^*\ddot{u} = -\frac{ne^2}{\epsilon_0\epsilon_\infty}u,$$

$$\omega_p^2 = \frac{ne^2}{m^*\epsilon_0\epsilon_\infty}.$$

In a homogeneous bulk the same long-wavelength mode follows from continuity, carrier momentum and Gauss's law for a longitudinal density fluctuation. A longitudinal self-sustaining oscillation occurs at a zero of the dielectric function. With damping time τ the relative permittivity in this model is $\epsilon(\omega) = \epsilon_\infty[1 - \omega_p^2/(\omega(\omega + i/\tau))]$ for $e^{-i\omega t}$. Electron energy loss is sensitive to $-\mathrm{Im}(1/\epsilon)$, while transmission also depends on interfaces.

For $n = 10^{24}$ m⁻³, $m^* = 0.20m_e$ and $\epsilon_\infty = 12$, the model gives $\omega_p \simeq 3.64 \times 10^{13}$ rad/s, or 5.80 THz. Four times the density doubles this frequency if mass and background screening are unchanged.

Solve an effective electron–hole relative-coordinate problem

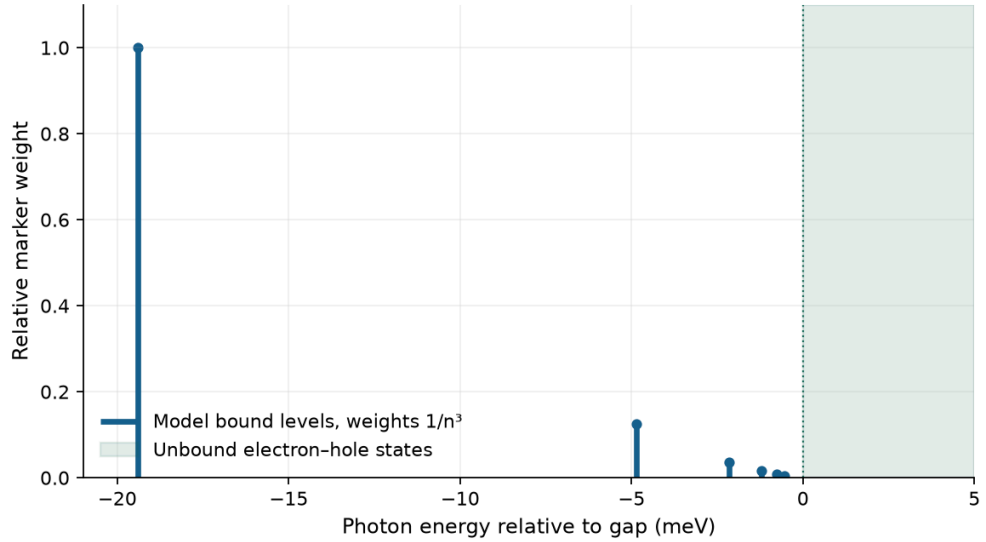
In a three-dimensional direct-gap semiconductor a photon can create a conduction electron and a valence hole. Separate their centre of mass from their relative coordinate. Near parabolic band edges the relative mass obeys $\mu^{-1} = 1/m_e^* + 1/m_h^*$. Approximate screening by a constant ϵ_r over the length and time scales of the pair. The relative Hamiltonian is then hydrogenic.

$$H_{\mathrm{rel}} = -\frac{\hbar^2\nabla^2}{2\mu} - \frac{e^2}{4\pi\epsilon_0\epsilon_r r},$$

$$E_n = E_g - \frac{R^*}{n^2}.$$

Minimising the expectation for an exponential radius a gives kinetic energy $\hbar^2/(2\mu a^2)$ and potential $-e^2/(4\pi\epsilon_0\epsilon_r a)$. The minimum yields $a^* = (\epsilon_r m_e/\mu)a_0$ and $R^* = (\mu/m_e)13.606\,\mathrm{eV}/\epsilon_r^2$. With $m_e^* = 0.20m_e$, $m_h^* = 0.50m_e$, $\epsilon_r = 10$, these give $\mu = 0.1429m_e$, $a^* = 3.70$ nm and $R^* = 19.4$

meV. The most strongly bound line lies this distance below the unbound continuum. A large radius relative to the unit cell supports the effective-mass model. A sub-gap peak alone can also come from a defect.



A hydrogenic bound series with a 19.4 meV exciton Rydberg approaches the continuum from below. Marker weights use the illustrative direct-transition envelope law proportional to the inverse cube of the level index. Broadening is omitted.

Try it · Exciton

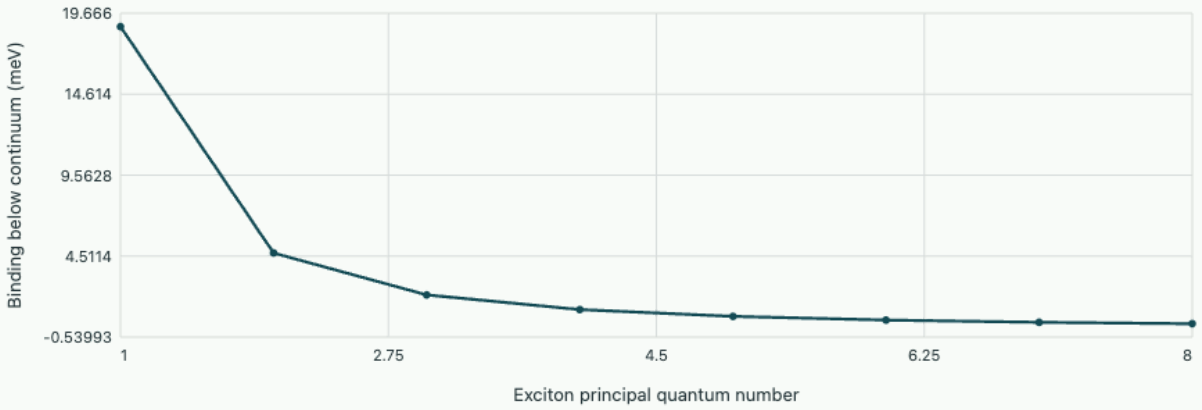
Change the inputs and compare the recalculated curves with the preceding derivation and baseline figure. The axes give the units; the numerical readout states the model assumptions and any limiting cases. Reset the inputs to return to the reference setting.

Open this live calculation

Try the calculation

Reduced electron-hole mass / electron mass **0.1**

Relative permittivity **8.5**



Hydrogenic exciton series

Effective Rydberg 18.831 meV; effective Bohr radius 4.498 nm. Effective-mass and dielectric screening approximations require a sufficiently extended exciton.

Let a single carrier relax a lattice coordinate

Take a local displacement Q_i, stiffness K, and local occupation n_i. Each site's lattice energy and coupling are $KQ_i^2/2 - gQ_i n_i$. At a fixed occupation distribution minimise over each displacement. In the adiabatic classical distortion model,

$$Q_i = g n_i / K,$$

$$E_{\mathrm{relax}} = -\frac{g^2}{2K} \sum_i n_i^2.$$

A carrier with all its weight on one site gains $g^2/(2K)$. With uniform weight across N sites the gain is smaller by N. Hopping competes with this localisation energy. For $g = 2.0$ eV/nm and $K = 20$ eV/nm² the one-site relaxation is 0.10 eV and the optimum displacement 0.10 nm. Compare with the bandwidth

before concluding that a small polaron will form. Quantised phonons, tunnelling of the distortion and long-range polar coupling are additional physics.

> **Recall · Screening has a frequency scale**
>
> A bound pair and a fast plasma oscillation need not see the same dielectric constant. Identify which lattice and electronic modes can follow each perturbation before importing a tabulated static permittivity.

Tutorial on assigning a measured feature

1 · Extract an exciton binding scale from two lines

▼ Work through the solution

In the hydrogenic series $E_2 - E_1 = 3R^*/4$. A splitting of 12 meV gives $R^* = 16$ meV and continuum $E_g = E_1 + 16$ meV. Check another member or the absorption onset to distinguish an accidental pair of defect peaks.

---

2 · Separate two density dependencies

▼ Work through the solution

A mode increasing from 5.8 to 8.2 THz as the carrier density doubles follows the plasmon square-root trend. The simple isolated exciton model has no such density law. At high density screening or many-body effects can also modify the exciton spectrum.

---

3 · Test the localisation argument

▼ Work through the solution

For equal occupation of two sites the distortion energy gain is half the one-site gain. A two-site bonding state can lower the electronic kinetic energy by a hopping energy t. If t is large compared with the difference in relaxation energies, localisation cannot be inferred from the static distortion gain alone.

For further study see Kittel, Introduction to Solid State Physics, 8th edition, chapters 14–15 on collective excitations, polarons and optical response.

Structure, excitations and probes of solids · 12. Ferromagnetic resonance from angular momentum and free-energy curvature

A uniformly magnetised thin specimen can absorb microwave power at a frequency far from the bare spin Larmor frequency. The precessing magnetic moment creates its own field. Its geometry and the anisotropy determine which restoring torques appear in the measured resonance.

Linearise the torque around the equilibrium orientation

Consider a saturated, uniformly magnetised ellipsoid with equilibrium along x. Write the dimensionless unit magnetisation as $\mathbf{m} \simeq (1, m_y, m_z)$. To second order use a free energy density $F = F_0 + M_s(B_y m_y^2 + B_z m_z^2)/2$ with both curvature fields positive in tesla. They include bias, demagnetising fields and anisotropy. A small applied microwave field $b_y(t)$ adds $-M_s b_y m_y$. Define the effective field by $-\partial F/\partial \mathbf{m}$ divided by M_s.

$$\dot{\mathbf{m}} = -\gamma\, \mathbf{m} \times \mathbf{B}_{\mathrm{eff}},$$

$$\dot{m}_y = -\gamma B_z m_z,$$

$$\dot{m}_z = \gamma B_y m_y - \gamma b_y.$$

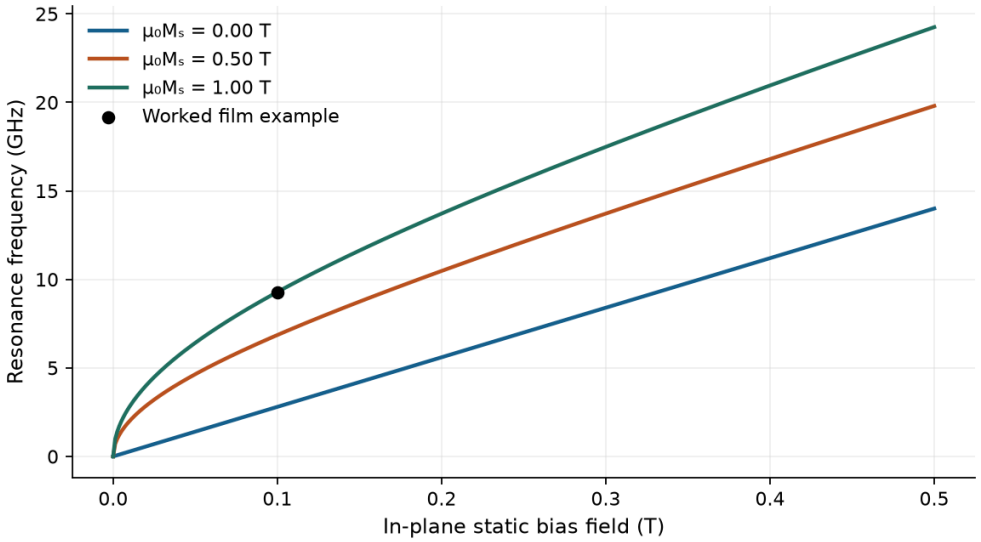
Differentiating the first equation and eliminating m_z gives $\ddot{m}_y + \gamma^2 B_y B_z m_y = \gamma^2 B_z b_y$. The free precession frequency is $\omega_0 = \gamma\sqrt{B_y B_z}$. The orbit generally has unequal semiaxes. In the limit of equal curvature fields the circular bare-spin result is recovered.

Obtain the thin-film frequency in an in-plane field

In a wide thin film, uniform in-plane rotation creates little demagnetising field. An out-of-plane tilt costs approximately $\mu_0 M_s^2 m_z^2/2$. A bias B_0 contributes $-M_s B_0 m_x \simeq -M_s B_0 + M_s B_0(m_y^2 + m_z^2)/2$. Neglect crystalline anisotropy and edge corrections. Thus $B_y = B_0$ and $B_z = B_0 + \mu_0 M_s$. With $\gamma/(2\pi) = 28$ GHz/T, $\mu_0 M_s = 1.00$ T and $B_0 = 0.10$ T we predict $f_0 = 9.29$ GHz. Using $28 B_0$ alone would give 2.80 GHz.

Recall · Compare B-like and H-like parameters consistently

In these formulas all stiffness fields are in tesla and γ is in radians per second per tesla. If a field is in A/m it must first be converted where appropriate with μ_0. The static demagnetising field depends on shape as well as material.



The bare-spin straight line is recovered when the magnetisation contribution to the restoring field vanishes. An in-plane saturated film develops a curved frequency response.

Try it · Fmr

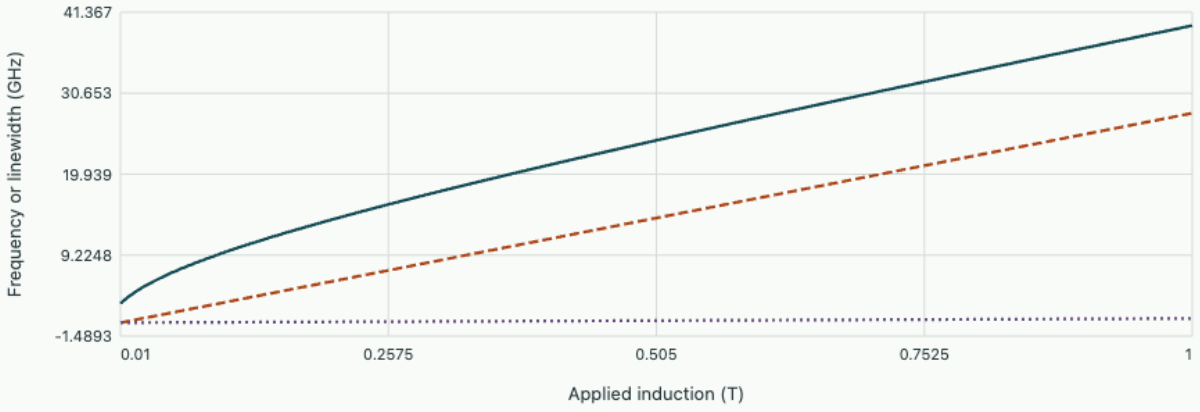
Change the inputs and compare the recalculated curves with the preceding derivation and baseline figure. The axes give the units; the numerical readout states the model assumptions and any limiting cases. Reset the inputs to return to the reference setting.

Open this live calculation

Try the calculation

Saturation induction μ0M (T) **1**

Gilbert damping α **0.01**



In-plane film resonance · Bare spin · Weak-damping FWHM

Gyromagnetic ratio / 2π = 28 GHz/T. Uniform saturated film, in-plane field, no extra anisotropy; linewidth is the weak-damping estimate.

Derive the absorbed-power peak and its width

Gilbert damping adds $+\alpha \mathbf{m} \times \dot{\mathbf{m}}$ to the torque equation. To first order in small α one obtains the damped denominator $\omega_0^2 - \omega^2 - i\alpha\gamma(B_y + B_z)\omega$. With convention $e^{-i\omega t}$ the average loss from a real drive of complex amplitude b is proportional to $\omega\ \mathrm{Im}(\chi)|b|^2/2$. Near resonance the absorptive susceptibility has a Lorentzian line shape. Its angular-frequency full width at half maximum to this order is

$$\Delta\omega_{\mathrm{FWHM}} \simeq \alpha\gamma(B_y + B_z).$$

For the model film at $B_0 = 0.10$ T and $\alpha = 0.010$ the frequency-swept width is about 0.336 GHz. A field-swept experiment must divide the frequency width by $|df_0/dB_0|$ and distinguish the width of the absorption peak from a derivative peak-to-peak linewidth. Inhomogeneous fields and mode overlap broaden real lines as well.

Tutorial on extracting magnetic parameters

1 · Recover a saturation magnetisation

▼ Work through the solution

For an in-plane film at 0.12 T, a uniform resonance at 10.0 GHz gives $\mu_0 M_s = (10/28)^2/0.12 - 0.12 = 0.943$ T in this approximation. Repeating the measurement at several fields tests the assumed geometry.

---

2 · Infer an intrinsic damping estimate

▼ Work through the solution

For curvature fields 0.20 and 1.20 T and a 0.392 GHz full width, $\alpha \simeq 0.392/[28(1.40)] = 0.0100$. A field-independent broadening that also contributes to the observed width would bias this single-frequency estimate upward.

---

3 · Explain a soft mode

▼ Work through the solution

As one curvature approaches zero at a loss of equilibrium stability, the predicted restoring frequency approaches zero while the other curvature can remain finite. A broad or shifted low-frequency peak calls for checking domains and the validity of the uniform-magnetisation assumption.

For further study see Kittel, Introduction to Solid State Physics, 8th edition, chapters 11–13 on collective magnetic response and magnetic resonance.

Structure, excitations and probes of solids · 13. Lattice dislocations and structure without long-range order

A missing atom, a slipped lattice plane and a glass can all broaden a measurement, through very different mechanisms. Geometry distinguishes a line defect from a local vacancy. Correlation functions make the distinction between short-range order and crystallinity quantitative.

Construct a Burgers circuit and the field of a screw dislocation

Follow a closed sequence of lattice steps around a suspected defect, well outside its core. Repeat the same sequence in a perfect reference lattice. The closure failure defines the Burgers vector $\mathbf{b}$ up to the agreed sense of the circuit and line orientation. Its component parallel to the dislocation line is screw character and its perpendicular component is edge character. Smooth elastic deformation without a dislocation gives no persistent closure failure.

For a straight screw line along z, with Burgers magnitude b along z, an elastic displacement outside the core is $u_z = b\phi/(2\pi)$ in cylindrical coordinates. After one revolution the displacement changes by b. The engineering shear is $\gamma_{\phi z} = r^{-1}\partial_\phi u_z = b/(2\pi r)$, giving $\sigma_{\phi z} = \mu b/(2\pi r)$. Integrating the energy density $\mu\gamma^2/2$ in an annulus gives an energy per unit line length

$$\frac{E}{L} = \int_{r_c}^{R} \frac{\mu}{2}\left(\frac{b}{2\pi r}\right)^2 2\pi r\, dr = \frac{\mu b^2}{4\pi}\ln(R/r_c).$$

The core radius limits continuum elasticity at small radius. Nearby defects or surfaces set the outer cutoff. For $\mu = 30$ GPa, $b = 0.25$ nm and $R/r_c = 10^4$, the elastic term is 1.37×10^{-9} J/m. A core energy must be added to infer formation energies.

Determine how an applied shear does work on a line

A dislocation of length L moving a distance dx sweeps area Ldx. Across the swept area the material slips by b. A resolved shear stress τ supplies work $\tau b L dx$, hence the glide force per unit length is τb. At $\tau = 20$ MPa and $b = 0.25$ nm this gives 5.0×10^{-3} N/m. Obstacles and other dislocations oppose this driving force. Diffusion-assisted climb exchanges atoms or vacancies and depends on temperature in a different way.

> **Recall · Edge dislocations affect the number of planes**
>
> In an edge geometry the terminating extra half-plane ends at the dislocation line. A vacancy has no Burgers vector around a sufficiently large circuit. Concentration alone cannot describe a line's orientation, connectivity and mobility.

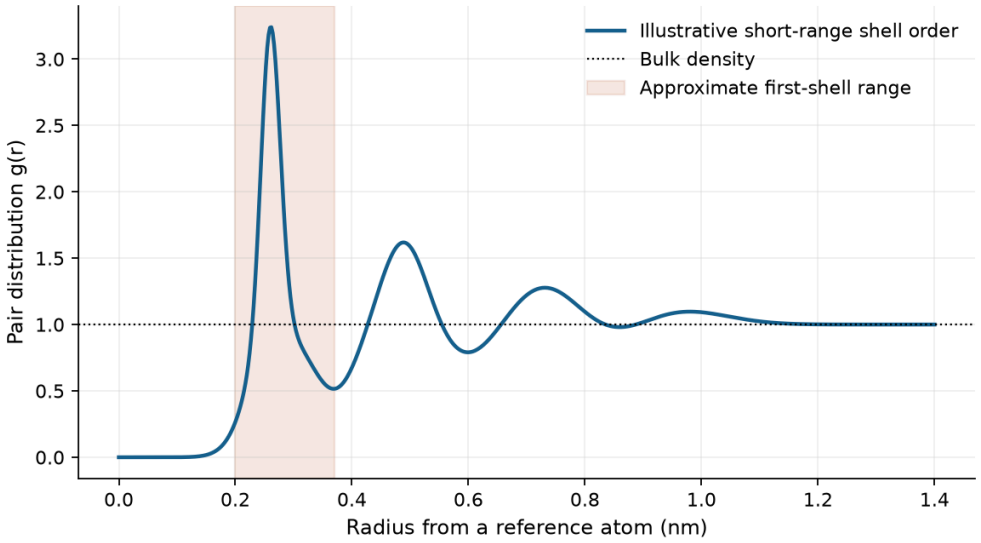
Recover pair order from scattering without indexing Bragg peaks

For particles of mean number density ρ, define $g(r)$ by the conditional count $dN = 4\pi r^2 \rho g(r)\, dr$ about an atom in an isotropic bulk sample. The first-shell coordination is the integral from the first-neighbour peak to its first minimum, including the correct r^2 weight. Scattering measures amplitudes before averaging the squared total. After averaging orientations the pair phase factor becomes $\sin(qr)/(qr)$.

$$S(q) = 1 + 4\pi\rho \int_0^\infty [g(r) - 1] \, \frac{\sin(qr)}{qr} \, r^2 dr.$$

A glass may have a sharp first-neighbour peak and further damped shells with $g(r) \to 1$. This permits strong local coordination without periodic translational order. An ideal crystal produces Bragg peaks in reciprocal space. A limited sample size or instrumental resolution also broadens crystalline peaks. Compare several peak widths and a real-space correlation length before assigning amorphous structure.

A glass transition is observed when a structural relaxation time becomes comparable to a measurement or cooling time. A slower scan permits structural rearrangement to lower temperatures. The measured transition temperature may therefore shift with rate. The sharp equilibrium melting point of a pure crystal and the observed glass-transition interval answer different experimental questions.



Illustrative pair-correlation profile for an isotropic disordered solid. The shaded first shell gives a coordination number after weighting the curve by the spherical shell volume and density.

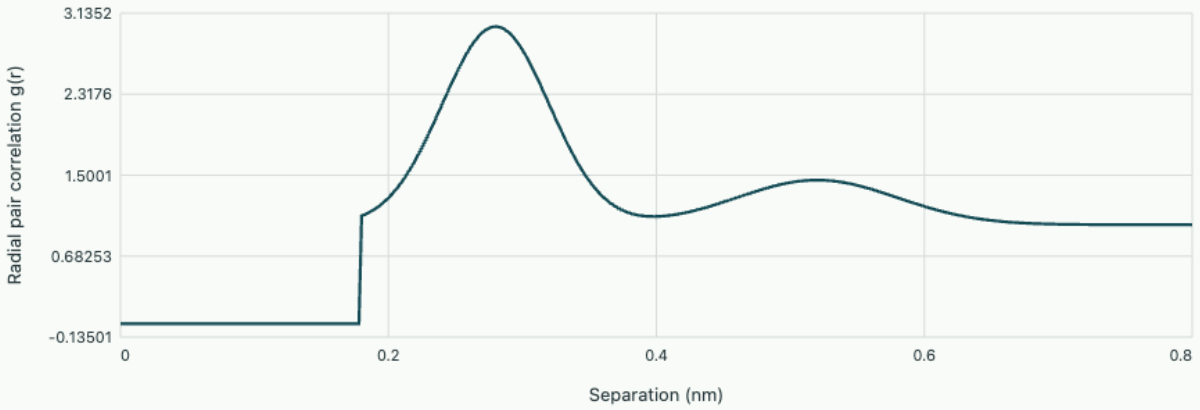
Try it · Pair order

Change the inputs and compare the recalculated curves with the preceding derivation and baseline figure. The axes give the units; the numerical readout states the model assumptions and any limiting cases. Reset the inputs to return to the reference setting.

Open this live calculation

Try the calculation

First-shell peak height	2
First-shell width (nm)	0.04
Number density (nm⁻³)	40



Illustrative disordered-solid pair correlation

Coordination integrated over 0.18–0.40 nm = 17.88. This adjustable phenomenological profile demonstrates shell-volume weighting; it is not a fitted material structure.

Tutorial on disorder measurements

1 · Identify a dislocation character

▼ Work through the solution

A line runs along z while the closure failure points along x. Its screw projection is zero, so the line is pure edge. An inclined segment on a curved line generally has mixed character even with the same conserved Burgers vector.

2 · Estimate a coordination number

▼ **Work through the solution**

Approximate a first shell by $g = 3$ between 0.23 and 0.27 nm with $\rho = 60$ nm⁻³ and zero elsewhere within that shell. Then $N = 4\pi\rho[0.27^3 - 0.23^3] \simeq 5.67$. Truncating below the first minimum or failing to subtract scattering backgrounds changes the estimate.

---

3 · Separate line broadening from amorphous order

▼ **Work through the solution**

A single broad powder maximum is insufficient. Examine whether higher peaks can be indexed on a consistent lattice, vary instrumental resolution, and estimate the range of oscillatory pair correlations. Compare thermal evolution and cooling-rate dependence for independent evidence.

For further study see Kittel, Introduction to Solid State Physics, 8th edition, chapters 19–21 on amorphous structure, point defects and dislocations.

Structure, excitations and probes of solids · 14. Why some alloys demix while others order on two sublattices

A binary alloy can cease to look random by separating into compositionally distinct regions or by arranging unlike atoms on alternating sites. A free energy for composition answers the first question. A second order parameter is needed for the second.

Count configurations and derive an energy of mixing

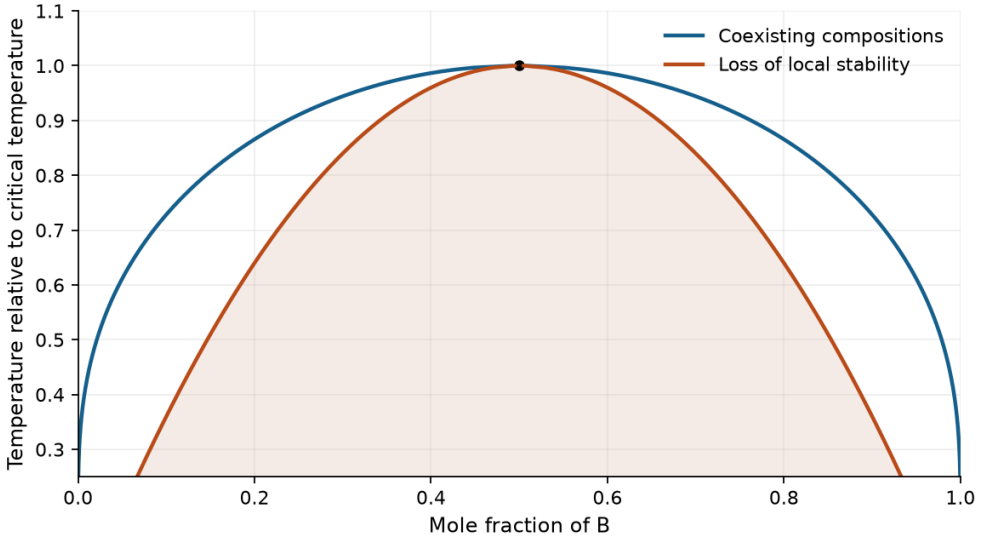
Let N lattice sites contain Nx atoms of B. The number of random arrangements is $N!/[(Nx)!(N(1-x))!]$. Stirling's approximation gives a configurational entropy per site $-k_B[x\ln x + (1-x)\ln(1-x)]$. In a random alloy each of $zN/2$ nearest-neighbour bonds is unlike with probability $2x(1-x)$. With one bond energy ϵ_{ij} per pair, subtract the energies of separated pure phases at the same overall composition.

$$\Omega = z\,[\epsilon_{AB} - (\epsilon_{AA} + \epsilon_{BB})/2],$$

$$\Delta g = \Omega x(1-x) + k_B T[x\ln x + (1-x)\ln(1-x)].$$

For $\Omega > 0$, unlike neighbours cost energy. The curvature at fixed temperature is $g'' = -2\Omega + k_B T/[x(1-x)]$. A homogeneous state is locally unstable when this curvature is negative. Equal chemical potentials across coexisting phases give a common tangent to $g(x)$. For the symmetric model $x_2 = 1 - x_1$, the tangent is horizontal and the binodal obeys $\Omega(1-2x) + k_B T \ln[x/(1-x)] = 0$.

At $x = 1/2$ the spinodal reaches its highest temperature $T_c = \Omega/(2k_B)$. For $\Omega = 0.10$ eV the mean-field T_c is 580 K. At 400 K the spinodal satisfies $x(1-x) = 0.1723$, or $x \simeq 0.221$ and 0.779. A composition between the binodal and spinodal can still have a positive local curvature while phase separation would lower the total energy after nucleation.



Coexistence compositions and local stability limits for the symmetric regular-solution model. A homogeneous mixture between these curves needs an initial fluctuation large enough to nucleate the competing phases.

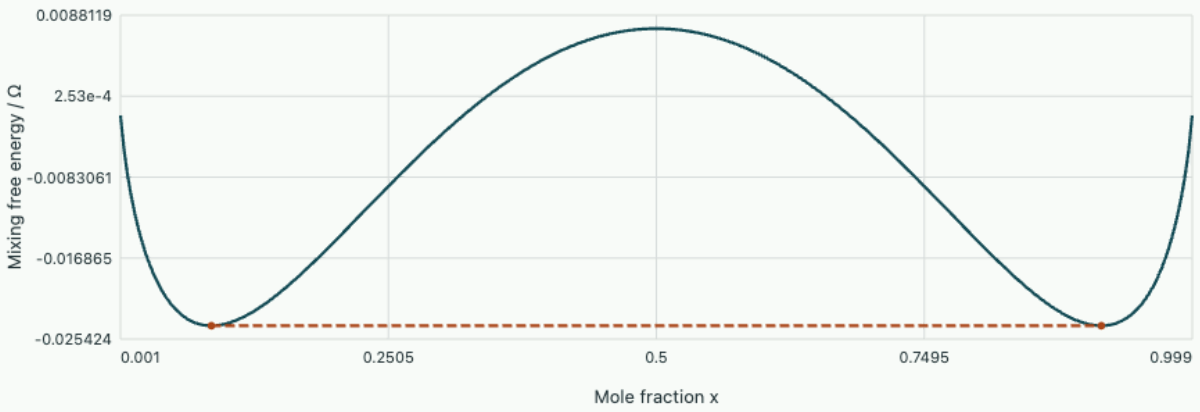
Try it · Regular solution

Change the inputs and compare the recalculated curves with the preceding derivation and baseline figure. The axes give the units; the numerical readout states the model assumptions and any limiting cases. Reset the inputs to return to the reference setting.

Open this live calculation

Try the calculation

Reduced temperature T/Tc **0.7**



Regular-solution free energy Common tangent

Binodal compositions 0.085683, 0.91432; spinodal 0.22614, 0.77386.

Construct an order parameter for preferential unlike neighbours

For an equiatomic alloy on a bipartite lattice let the A fractions of the two sublattices be $(1+\eta)/2$ and $(1-\eta)/2$. Then $\eta = 0$ is a random occupation and $|\eta| = 1$ is perfect order. Assuming independent occupation within each sublattice, the probability of an unlike nearest-neighbour bond is $(1+\eta^2)/2$. Put $w = \epsilon_{AB} - (\epsilon_{AA} + \epsilon_{BB})/2$. The energy change from the random state is $zw\eta^2/4$. Adding both sublattice mixing entropies gives the leading free-energy terms

$$g(\eta) - g(0) = \left(\frac{zw}{4} + \frac{k_B T}{2}\right)\eta^2 + \frac{k_B T}{12}\eta^4 + O(\eta^6).$$

For $w < 0$ the energetic gain favours order below $T_{\mathrm{ord}} = -zw/(2k_B)$. Domains can choose opposite signs and have the same composition. A superlattice diffraction reflection weights the difference of sublattice scattering amplitudes. Its amplitude is proportional to $(f_A - f_B)\eta$, so its ideal intensity scales as η^2. A measurement of the average composition alone overlooks the transition.

Recall · What makes this a mean-field model?

The product of single-site probabilities omits short-range correlations between neighbours. Clustering can therefore precede macroscopic separation and diffuse scattering can precede a sharp superlattice peak. Long-range elastic effects, unequal sublattice sizes or composition-dependent strain modify these predictions.

Distinguish an equilibrium phase boundary from slow atomic exchange

Composition changes by transport, which conserves the total fraction of each species. In a weak composition gradient a mobility $M > 0$ gives a flux proportional to $-\nabla\mu$ with $\mu = \partial g/\partial x$ in a locally uniform approximation. Negative curvature can drive atoms uphill in composition, amplifying fluctuations. A positive interfacial penalty proportional to $|\nabla x|^2$ prevents indefinitely fine segregation. In ordering at fixed composition, local exchanges can develop alternating occupation without transporting a macroscopic excess from one end of a specimen to the other.

Tutorial on alloy diffraction and stability

1 · Determine the sign of the interaction

▼ **Work through the solution**

If unlike bonds are 10 meV lower than the average like bond and coordination is eight, $w = -0.010$ eV gives a mean-field ordering temperature of $0.080/(2k_B) = 464$ K on a suitable bipartite lattice. Demixing is disfavoured in this nearest-neighbour calculation.

---

2 · Infer an order parameter

▼ **Work through the solution**

A superlattice reflection has one quarter of its intensity in a perfectly ordered single domain after correcting for geometry and thermal motion. The inferred $|\eta|$ is 0.5. Unequal domain volumes or poor scattering contrast demand a more complete intensity model.

---

3 · Diagnose two microstructures with similar average composition

▼ **Work through the solution**

In an equiatomic sample, composition mapping that resolves B-rich and A-rich regions indicates separation. Alternating-site superlattice peaks at essentially uniform local composition indicate ordering. Simultaneous data help when both mechanisms occur on different length scales.

For further study see Kittel, Introduction to Solid State Physics, 8th edition, chapter 22 on alloys and ordered structures.

Structure, excitations and probes of solids · 15. What extremal Fermi-surface orbits reveal about a metal

A single magnetic oscillation frequency gives one area in reciprocal space. Many different surfaces can share that area. Rotating the field and following how quantum oscillations and conductivity change turns the measurement into a three-dimensional inference problem.

Derive the plane of motion and the measured cross section

For semiclassical electrons of band energy $\epsilon(\mathbf{k})$ in a uniform static magnetic field with zero applied electric field, $\dot{\mathbf{r}} = \nabla_{\mathbf{k}}\epsilon/\hbar$ and $\hbar\dot{\mathbf{k}} = -e\dot{\mathbf{r}} \times \mathbf{B}$. Dotting the second equation with $\mathbf{B}$ shows that the orbit stays in a fixed plane perpendicular to the field. Dotting with $\nabla_{\mathbf{k}}\epsilon$ also shows that it remains on a constant-energy surface. A degenerate metal probes the intersection of these two surfaces near the Fermi level.

For a closed orbit of area $A(E, k_{\parallel})$ the semiclassical area quantisation condition is $A = 2\pi eB(n+\gamma)/\hbar$. At fixed Fermi energy adjacent crossings at increasing $1/B$ then have spacing $2\pi e/(\hbar A)$. Bulk signals sum oscillations from many neighbouring planes. Rapid phase variation cancels most contributions on averaging, leaving extrema of A along $k_{\parallel}$ particularly visible.

$$F = \frac{\hbar}{2\pi e} A_{\mathrm{ext}},$$

$$m_c = \frac{\hbar^2}{2\pi}\frac{\partial A}{\partial E}\bigg|_{\mathrm{orbit}}.$$

The second relation follows by differentiating the area quantisation with respect to energy and comparing successive-level spacing to $\hbar eB/m_c$. A measured area does not by itself give its energy derivative. Temperature damping or an independent mass measurement contains additional information.

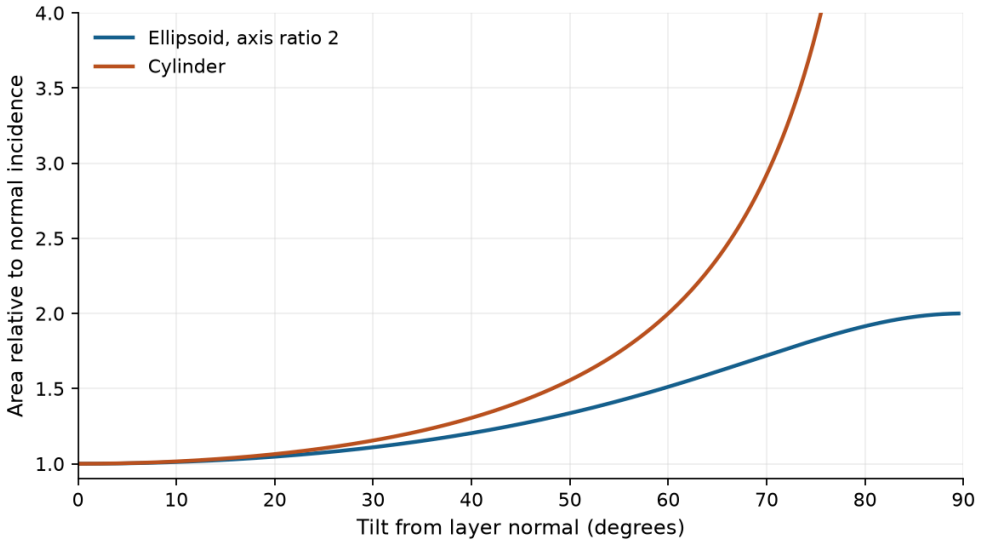
Predict the angular dependence for two competing surfaces

For an ellipsoid of semiaxes a, b, c in wave-number units, a linear scaling from a unit sphere gives a central section normal to $\mathbf{n}$ of area $\pi abc/\sqrt{a^2n_x^2 + b^2n_y^2 + c^2n_z^2}$. One way to see the denominator is to take a thin slab bounded by parallel planes. Under the inverse scaling the distance between the transformed planes changes by the inverse magnitude of the scaled normal. Equating volume before and after the transformation fixes the area factor.

For an axially symmetric ellipsoid take $a = b$ and tilt the field through angle θ from z. A circular cylinder of radius a instead has section area $\pi a^2/|\cos\theta|$ so long as a closed orbit exists. At normal incidence both predict the same frequency. For $c = 2a$, the ellipsoid predicts $F(60^\circ)/F(0) = 2/\sqrt{0.75+1} = 1.512$, while the cylinder predicts 2. An ellipsoid closes with a finite side-on area. A perfectly unwarped cylinder has open trajectories for a field in its plane.

Recall · Open orbits in a periodic crystal

In a reduced-zone drawing a trajectory can reappear at the opposite zone edge. Unfold the reciprocal lattice to see whether it closes or runs through successive zones. Such open orbits do not give an ordinary closed-area oscillation frequency and can strongly affect anisotropic transport.



An elongated ellipsoid and a cylinder agree for a field normal to the layers. Their extremal areas separate markedly as the field rotates toward the layer plane.

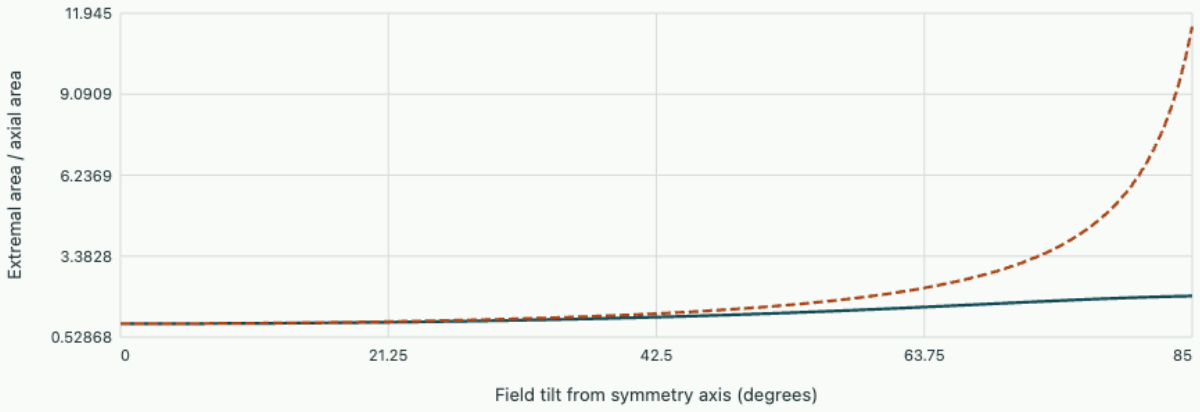
Try it · Fermi area

Change the inputs and compare the recalculated curves with the preceding derivation and baseline figure. The axes give the units; the numerical readout states the model assumptions and any limiting cases. Reset the inputs to return to the reference setting.

Open this live calculation

Try the calculation

Ellipsoid polar / equatorial radius 2



Onsager frequency scales with the plotted area. An ellipsoid remains bounded at 90°; a perfect cylinder diverges in this ideal geometry.

Allow necks, multiple sheets and unequal visibility

A weakly warped quasi-two-dimensional sheet can have a belly and a neck. Model their areas as $A_0(1+\eta)$ and $A_0(1-\eta)$ for field along the layer normal. Then $F_0 = (F_b + F_n)/2$ and $\eta = (F_b - F_n)/(F_b + F_n)$. For 500 and 440 tesla, these give 470 tesla and a relative corrugation of 0.0638. With similar amplitudes the sum of the two oscillations contains an envelope $\cos[\pi(F_b - F_n)/B]$. The spacing of successive envelope nodes in inverse field is $1/|F_b - F_n|$.

Several frequencies can instead come from different electron and hole pockets. Measure the angular branches continuously and compare their effective masses, crystal symmetry and independent Hall and transport data. A heavy or strongly scattered orbit may be too weak to see. Assigning the entire carrier density to the most visible frequency can miss whole sheets. For an isotropic band with a spherical spin-degenerate pocket, the additional geometric assumption gives $n = k_F^3/(3\pi^2)$. Its boundary should be stated when reporting a density.

Tutorial on competing metal models

1 · Convert an oscillation frequency to an area

▼ **Work through the solution**

At $F = 500$ T, $A = (2\pi e/\hbar)F = 4.77 \times 10^{18}$ m⁻². If the orbit is circular the radius is $\sqrt{A/\pi} = 1.23 \times 10^{9}$ m⁻¹. The first number follows without assuming a circular shape.

---

2 · Estimate a beat period

▼ **Work through the solution**

With the two measured frequencies separated by 60 T, successive envelope zeros are separated by 0.0167 T⁻¹. A recording window of only 0.005 T⁻¹ cannot resolve the splitting convincingly. Vary the inverse-field window and check harmonic peaks.

---

3 · Infer an ellipsoid axis ratio from a side-on rotation

▼ **Work through the solution**

For $a = b$ the side-on to normal frequency ratio of a closed ellipsoid is c/a. A ratio 1.7 implies $c/a = 1.7$. If the signal disappears before reaching side-on, the missing end point leaves this inference underdetermined. Seek independent sections or a second rotation plane.

For further study see Kittel, Introduction to Solid State Physics, 8th edition, chapters 6–9 on electrons in metals, band structure and Fermi surfaces.